Atmos. Chem. Phys., 21, 14333–14349, 2021
https://doi.org/10.5194/acp-21-14333-2021

Atmospheric Chemistry and Physics
Open Access

Impact of pyruvic acid photolysis on acetaldehyde and peroxy radical formation in the boreal forest: theoretical calculations and model results

Philipp G. Eger[1], Luc Vereecken[2], Rolf Sander[1], Jan Schuladen[1], Nicolas Sobanski[1], Horst Fischer[1], Einar Karu[1], Jonathan Williams[1], Ville Vakkari[3,4], Tuukka Petäjä[5], Jos Lelieveld[1], Andrea Pozzer[1], and John N. Crowley[1]

[1]Atmospheric Chemistry Department, Max-Planck-Institute for Chemistry, 55128 Mainz, Germany
[2]Institute for Energy and Climate Research: IEK-8, Forschungszentrum Juelich, 52425 Juelich, Germany
[3]Atmospheric Composition Unit, Finnish Meteorological Institute, 00101 Helsinki, Finland
[4]Atmospheric Chemistry Research Group, Chemical Resource Beneficiation,
North-West University, Potchefstroom, South Africa
[5]Institute for Atmospheric and Earth System Research (INAR)/Physics,
Faculty of Science, University of Helsinki, Helsinki, Finland

Correspondence: John N. Crowley (john.crowley@mpic.de)

Received: 18 September 2020 – Discussion started: 20 October 2020
Revised: 1 September 2021 – Accepted: 7 September 2021 – Published: 28 September 2021

Abstract. Based on the first measurements of gas-phase pyruvic acid ($CH_3C(O)C(O)OH$) in the boreal forest, we derive effective emission rates of pyruvic acid and compare them with monoterpene emission rates over the diel cycle. Using a data-constrained box model, we determine the impact of pyruvic acid photolysis on the formation of acetaldehyde (CH_3CHO) and the peroxy radicals $CH_3C(O)O_2$ and HO_2 during an autumn campaign in the boreal forest.

The results are dependent on the quantum yield (φ) and mechanism of the photodissociation of pyruvic acid and the fate of a likely major product, methylhydroxy carbene (CH_3COH). With the box model, we investigate two different scenarios in which we follow the present IUPAC (IUPAC Task Group on Atmospheric Chemical Kinetic Data Evaluation, 2021) recommendations with $\varphi = 0.2$ (at 1 bar of air), and the main photolysis products (60 %) are acetaldehyde + CO_2 with 35 % C–C bond fission to form HOCO and CH_3CO (scenario A). In the second scenario (B), the formation of vibrationally hot CH_3COH (and CO_2) represents the main dissociation pathway at longer wavelengths (∼ 75 %) with a ∼ 25 % contribution from C–C bond fission to form HOCO and CH_3CO (at shorter wavelengths). In scenario 2 we vary φ between 0.2 and 1 and, based on the results of our theoretical calculations, allow the thermalized CH_3COH to react with O_2 (forming peroxy radicals) and to undergo acid-catalysed isomerization to CH_3CHO.

When constraining the pyruvic acid to measured mixing ratios and independent of the model scenario, we find that the photolysis of pyruvic acid is the dominant source of CH_3CHO with a contribution between ∼ 70 % and 90 % to the total production rate. We find that the photolysis of pyruvic acid is also a major source of the acetylperoxy radical, with contributions varying between ∼ 20 % and 60 % dependent on the choice of φ and the products formed. HO_2 production rates are also enhanced, mainly via the formation of CH_3O_2. The elevated production rates of $CH_3C(O)O_2$ and HO_2 and concentration of CH_3CHO result in significant increases in the modelled mixing ratios of $CH_3C(O)OOH$, CH_3OOH, HCHO, and H_2O_2.

1 Introduction

Organic acids play a crucial role in tropospheric chemistry, impacting secondary organic aerosol formation, air quality, and climate (Kanakidou et al., 2005; Hallquist et al., 2009). Pyruvic acid ($CH_3C(O)C(O)OH$), an organic acid that is central in plant metabolism as part of the Krebs cycle

Published by Copernicus Publications on behalf of the European Geosciences Union.

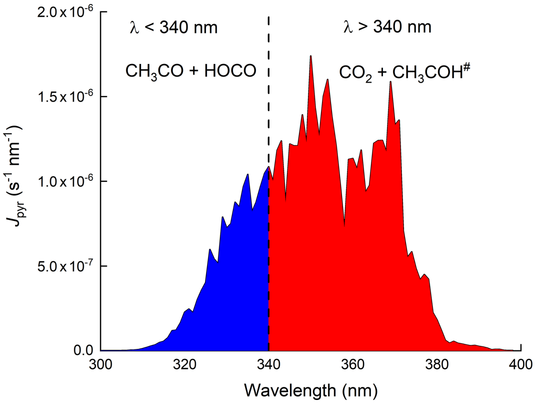

Figure 1. Wavelength-resolved photolysis rates (J_{pyr}) for 13 September 2016 at solar noon. J_{pyr} was calculated using a photolysis quantum yield of 1 and the absorption cross sections at 298 K preferred by IUPAC Task Group on Atmospheric Chemical Kinetic Data Evaluation (2021).

(Walker, 1962), is found in tropospheric air in the gas phase as well as in the aerosol phase, especially in the boundary layer over vegetated regions. Gas-phase mixing ratios ranging from a few to several hundred parts per trillion (pptv) have been reported in various locations around the world, including the tropical rainforest, boreal forest, rural areas with temperate forest, and regions influenced by urban outflow. A recent overview of existing measurements of gas-phase pyruvic acid is given by Eger et al. (2020).

A known source of pyruvic acid is the photo-oxidation of isoprene, via the ozonolysis of methyl vinyl ketone and subsequent hydrolysis of the Criegee intermediates (Jacob and Wofsy, 1988; Grosjean et al., 1993; Paulot et al., 2009). Further potential sources are the photolysis of methylglyoxal (Raber and Moortgat, 1995), the gas-phase photo-oxidation of aromatics in the presence of NO_x (Grosjean, 1984; Praplan et al., 2014), the aqueous-phase oxidation of methylglyoxal (Stefan and Bolton, 1999), and reactions taking place within biomass burning plumes (Andreae et al., 1987; Helas et al., 1992). In addition, pyruvic acid has been reported to be directly emitted from vegetation (Talbot et al., 1990; Jardine et al., 2010a, b; Eger et al., 2020). Compared to acetic acid, the presence of a second (non-acidic) carbonyl group imparts on pyruvic acid an absorption spectrum that extends from ultraviolet to visible wavelengths (see Fig. 1), and photolysis is a major sink of pyruvic acid in the boundary layer, with deposition and heterogeneous uptake to the aerosol phase also contributing to its removal. Photolysis of pyruvic acid in air results in a number of different radical and stable products; the major ones are expected to be acetaldehyde, HO_2, and $CH_3C(O)O_2$ (more details are presented in Sect. 1.1). These products can have a significant impact on tropospheric chemistry, e.g. via the formation of peroxyacetyl nitrate (PAN), peracetic acid, and formaldehyde (HCHO).

Global models have recently revealed discrepancies between simulated and measured acetaldehyde concentrations (Millet et al., 2010; Wang et al., 2019; Wang et al., 2020). Wang et al. (2020) reported CH_3CHO mixing ratios that were up to a factor of 10 higher than predicted by a global chemistry-transport model (EMAC) in the marine boundary layer around the Arabian Peninsula, implying missing sources of CH_3CHO in remote and polluted regions. Wang et al. (2019) also found that models systematically underestimate CH_3CHO compared to observations, implying a missing source of acetaldehyde in the remote troposphere. This finding was supported by the simultaneous measurement of peracetic acid (which is formed, for example, via the degradation of acetaldehyde in remote environments) with the organic aerosol source of CH_3CHO also being insufficient to explain the results. Instead, Wang et al. (2019) suggested that CH_3CHO arises from the degradation of gas-phase organic compounds. Pyruvic acid, among other organic acids in the gas and aerosol phase, might be one of the compounds that can be converted to acetaldehyde in the remote troposphere, and its integration into global models might contribute to resolve discrepancies, especially in forested regions.

Generally, field measurements as well as modelling and laboratory-based kinetic studies on pyruvic acid are limited, and its impact on atmospheric chemistry is still poorly understood. In this study we highlight the potential role of pyruvic acid in the boreal forest, one of the largest terrestrial biomes on Earth. For this, we use data from a measurement campaign in 2016 (IBAIRN, Influence of Biosphere–Atmosphere Interactions on the Reactive Nitrogen budget).

The photolysis of pyruvic acid: quantum yields and products

Because its reaction with OH is slow ($k_{\mathrm{OH+pyruvic\ acid}} = 1.2 \times 10^{-13}\ \mathrm{cm^3\ molecule^{-1}\ s^{-1}}$ at 298 K; Mellouki and Mu, 2003), photolysis and dry deposition are the dominant loss terms for gas-phase pyruvic acid. Heterogeneous uptake to atmospheric aerosols is also calculated to be inefficient during the IBAIRN campaign in the boreal forest (see below), where particle surface area densities were of the order of $2 \times 10^{-7}\ \mathrm{cm^2\ cm^{-3}}$, and the particles contained a large organic fraction (Liebmann et al., 2019) that is likely to reduce the uptake coefficient compared to that measured for pure aqueous particles ($\gamma = 0.06$; Eugene et al. 2018).

The photodissociation of pyruvic acid at actinic wavelengths is not well understood. According to the most recent IUPAC Task Group on Atmospheric Chemical Kinetic Data Evaluation (2021) evaluation, which considers experimental data until 2017, the three thermodynamically accessible photolysis channels are

$$CH_3C(O)C(O)OH + h\nu \rightarrow CH_3CHO + CO_2 \quad \text{(R1)}$$

$$\rightarrow CH_3C(O)OH + CO \quad \text{(R2)}$$

$$\rightarrow CH_3CO + HOCO. \quad \text{(R3)}$$

IUPAC recommends a photodissociation quantum yield (φ) of 0.2 at 1 bar pressure (i.e. for boundary layer conditions), with branching ratios of 0.6, 0.05, and 0.35 for Reactions (R1), (R2), and (R3), respectively, which implicitly assumes that the initially formed carbene (CH_3COH) immediately isomerizes to acetaldehyde. The radical products of Reaction (R3) (CH_3CO and HOCO) react rapidly in air to form peroxy radicals (Reactions R4 and R5).

$$CH_3CO + O_2 + M \rightarrow CH_3C(O)O_2 + M \quad \text{(R4)}$$

$$HOCO + O_2 \rightarrow HO_2 + CO_2 \quad \text{(R5)}$$

The formation of methylhydroxy carbene (CH_3COH) as an intermediate in pyruvic acid photolysis has been postulated for many years (Vesley and Leermakers, 1964; Yamamoto and Back, 1985). Schreiner et al. (2011) observed isomerization of singlet CH_3COH to acetaldehyde in an Ar matrix at 11 K; their high-level theoretical analysis revealed high barriers for isomerization, where H-atom tunnelling through the energy barrier led to a lifetime of about 1 h at 11 K, which favoured the formation of acetaldehyde over that of vinyl alcohol. Only very recently has CH_3COH been detected experimentally as a product of pyruvic acid photolysis in the gas-phase (Samanta et al., 2021) and its unimolecular isomerization to both CH_3CHO and $CH_2{=}CHOH$ confirmed to be efficient at the experimental pressure of a few millibars (mbar) of helium. Indeed, Samanta et al. (2021) show that, at a photolysis wavelength of 351 nm (close to the maximum cross-section of pyruvic acid) formation of an energy-rich carbene ($CH_3COH^{\#}$) and CO_2 (Reaction R6) is essentially the only product channel operating. CH_3CHO and $CH_2{=}CHOH$ were formed subsequently (at $\sim 2:1$ ratio favouring CH_3CHO) in the unimolecular isomerization of $CH_3COH^{\#}$ (Reactions R7 and R8).

$$CH_3C(O)C(O)OH + h\nu \rightarrow CH_3COH^{\#} + CO_2 \quad \text{(R6)}$$

$$CH_3COH^{\#} \rightarrow CH_3CHO \quad \text{(R7)}$$

$$\rightarrow CH_2{=}CHOH \quad \text{(R8)}$$

Samanta et al. (2021) suggest that, at ambient pressures, a significant fraction of the energized, nascent carbene will be deactivated by collisions with air (Reaction R9) and the thermalized carbene (CH_3COH), which can no longer rapidly overcome the barriers to isomerization, may react with oxygen or water vapour (Reed Harris et al., 2016, 2017b; Eger et al., 2020; Samanta et al., 2021) (Reactions R10 and R11).

$$CH_3COH^{\#} + M \rightarrow CH_3COH + M \quad \text{(R9)}$$

$$CH_3COH + O_2 \rightarrow CH_3C(O) + HO_2 \quad \text{(R10)}$$

$$CH_3COH + H_2O \rightarrow CH_3CH(OH)_2 \quad \text{(R11)}$$

As summarized by IUPAC, there have been many experimental studies deriving primary photodissociation quantum yields and product yields following the photolysis of pyruvic acid. The studies which were carried out at atmospherically relevant wavelengths (i.e. within the $\sim$ 300–400 nm absorption band) are listed in Table S1 in the Supplement. The experiments were carried out at different pressures of various bath gases and at different wavelengths and at different concentrations of pyruvic acid, all of which appear to play a role in determining the products formed. Table S1 shows that CO_2 is formed at a yield of close to 100 %, whereas the yield of CH_3CHO is highly variable. $CH_2{=}CHOH$ has been detected both at a few torr of helium (Samanta et al., 2021) and at 1 bar of air (Calvert et al., 2011). Other end products observed during the photolysis of pyruvic acid in 1 bar of air include acetic acid (Calvert et al., 2011; Reed Harris et al., 2016, 2017b) and PAN (Grosjean, 1983; Berges and Warneck, 1992) when NO_2 was present, which together provide evidence for the formation of the acetyl peroxy radical ($CH_3C(O)O_2$) and thus CH_3CO, for example, in Reactions (R3) and (R4) when sunlight or solar-simulating light sources are used. Secondary products (resulting, for example, from the further reactions of CH_3CHO) such as HCHO and CH_3OH have also been observed at pressures close to 1 bar (Grosjean, 1983; Calvert et al., 2011; Reed Harris et al., 2016; Reed Harris et al., 2017a). While the Norrish type 1 process (C–C bond fission) forming CH_3CO and HOCO appears to be unimportant at 351 nm (Samanta et al., 2021), it may be favoured at wavelengths < 340 nm (Chang et al., 2014). This is illustrated in Fig. 1 where we present the wavelength-resolved photolysis rate constants across the UV absorption spectrum of pyruvic acid (assuming an overall photolysis quantum yield of 1, and absorption cross-sections recommended by IUPAC). The wavelength-resolved actinic flux was calculated for the IBAIRN measurement site on the 13 September 2016 using the Tropospheric Ultraviolet and Visible Radiation model (TUV; https://www.acom.ucar.edu/Models/TUV/Interactive_TUV/, last access: 1 September 2020). Integration of the J values at wavelengths < 340 nm indicates that (at local noon) ≈ 25 % of pyruvic acid dissociation occurs at these shorter wavelengths.

2 Methods

The goal of this study is to evaluate the impact of pyruvic acid on acetaldehyde and radical formation rates in the boreal forest using a data-constrained, chemical box model. For this purpose we make use of experimental data from a field study, which was performed in the Finnish boreal forest at the Station for Measuring Ecosystem-Atmosphere Relations II (SMEAR II) in Hyytiälä (61.846° N, 24.295° E; 180 m above sea level; see Hari and Kulmala, 2005), an area that is characterized by large emission rates of biogenics (mainly monoterpenes) and low-NO_x concentrations (Rinne et al., 2000; Williams et al., 2011; Aalto et al., 2015; Fischer et al., 2021).

The variability in the reported photodissociation quantum yield and product distributions (see discussion above) suggests that pyruvic acid photodissociation is not yet fully understood, In addition, the fate of the potentially dominant carbene product (Samanta et al., 2021) is unknown. Therefore, in order to better constrain the fate of CH_3COH in the atmosphere, quantum chemical calculations were undertaken to characterize its likely atmospheric reactions, for which experimental data do not exist.

2.1 The IBAIRN campaign

The IBAIRN campaign took place in September 2016, during the summer–autumn transition, and was characterized by frequent temperature inversions near ground level during night-time (Liebmann et al., 2018a), which led to the accumulation of nocturnally emitted trace gases from vegetation. A detailed description of the campaign and the instruments deployed can be found elsewhere (Liebmann et al., 2018a; Eger et al., 2020). A summary (with details of detection limit, etc.) is provided in Table S2. Briefly, pyruvic acid was measured by a chemical ionization quadrupole mass spectrometer (Eger et al., 2020), the sum of monoterpenes (henceforth referred to as MT) was measured by a PTR-ToF-MS, and single MTs were monitored by a GC-AED (Liebmann et al., 2018a). Despite some discrepancies related to instrument location and inhomogeneity in terpene emissions within the forest, both instruments were in reasonably good agreement throughout the campaign. Since a high temporal resolution is preferable for our simulation, we have used the PTR-ToF-MS dataset. NO and NO_2 were measured by a chemiluminescence detector and a cavity ring-down spectrometer (Sobanski et al., 2016; Liebmann et al., 2018b), ozone was measured by optical absorption, and CO was measured by quantum-cascade-laser absorption spectroscopy (Eger et al., 2020). Formic and acetic acid as well as methyl ethyl ketone (MEK) and methyl vinyl ketone (MVK) were taken from the continuous PTR-MS measurements at the site at heights between 42 and 336 m. Photolysis rate coefficients were derived using actinic flux measurements from a spectral radiometer (METCON GmbH) (METCON GmbH) and evaluated cross sections and quantum yields (Burkholder et al., 2015). Mixing layer (MXL) heights were derived by combining in situ measurements made by a scanning Doppler lidar (Hellén et al., 2018) with results from the ECMWF ERA-Interim reanalysis (Dee et al., 2011), with a spatial resolution of ~ 80 km. Since the lidar was unable to resolve MXL heights < 60 m (as regularly experienced during nocturnal inversions), all values below this threshold have been set to 60 m, representing an upper limit.

2.2 Theoretical analysis of the fate of singlet methylhydroxy carbene, CH_3COH

We investigated the reactions of CH_3COH theoretically under atmospheric conditions, examining its unimolecular reactions and bimolecular reactions with O_2, H_2O, and HC(O)OH, where the latter is representative of carboxylic acids. The reaction with pyruvic acid itself is also briefly explored. The rovibrational characteristics and energetics of all critical points on the potential energy surface were characterized at the CCSD(T)/aug-cc-pVTZ//M06-2X-D3/aug-cc-pVTZ level of theory with a wavenumber scaling factor of 0.971 (Zhao and Truhlar, 2008; Dunning, 1989; Purvis and Bartlett, 1982; Grimme et al., 2011; Database of Frequency Scale Factors for Electronic Model Chemistries (Version 4); Alecu et al., 2010). This method compares favourably with the more rigorous focal point analysis of Schreiner et al. (2011), with energy differences in the singlet state unimolecular chemistry of less than 0.7 $\mathrm{kcal\,mol^{-1}}$, indicating that the method is reliable for kinetic predictions under atmospheric temperatures. Where necessary, broken-symmetry SCF (self-consistent field) calculations were used to describe singlet biradicals (Noodleman, 1981), and IRC (intrinsic reaction coordinate) calculations were used to verify the pathways. For reactants, products, and transition states, we exhaustively characterized all conformers; for complexes we only characterized those directly connecting to a transition state. All quantum chemical calculations were performed using the Gaussian-16 program suite (Frisch et al., 2016).

The quantum chemical data were then used to calculate high-pressure rate coefficients for reactions over a saddle point using multi-conformer transition state theory (MC-TST) calculations (Vereecken and Peeters, 2003), under a rigid rotor harmonic oscillator approximation. Tunnelling corrections are performed assuming an asymmetric Eckart barrier (Eckart, 1930; Johnston and Heicklen, 1962). Most reactions have high energy barriers, and the presence of pre- and post-reaction complexes has a negligible influence on the reaction rate. For barrierless reactions, typically complexation reactions, we assume the reaction rate is close to the collision limit unless indicated otherwise.

2.3 Box model

We have used the CAABA/MECCA atmospheric chemistry box model to numerically simulate the impact of pyruvic acid photolysis on the formation of radicals and CH_3CHO over the diel cycle during the IBAIRN campaign. Our study is based on model version 4.4.2, with updated reactions related to pyruvic acid in which two different scenarios were investigated (see Sect. 3.3) in order to examine the sensitivity of the model output to, for example, photolysis quantum yields and products.

The chemical mechanism used in this study contains >600 gas-phase species and ~ 2000 gas-phase reactions and photolysis steps. In addition to the basic ozone, HO_x and NO_x chemistry, the mechanism contains the detailed "Mainz Organic Mechanism" (MOM) for non-methane hydrocarbons (NMHC), isoprene, terpenes, and aromatics. MOM is derived from a reduced version of the Master Chemical Mechanism (MCM). Full details about CAABA/MECCA and MOM are available in Sander et al. (2019). Photolysis reactions are calculated for a latitude of 62° N. A complete reaction scheme and source of rate coefficients can be found in the data archive (see Data availability section).

Several parameters (temperature, pressure, relative humidity) and trace-gas concentrations (pyruvic acid, O_3, NO, NO_2, PAN, CO, MTs, formic and acetic acid, methyl ethyl ketone (MEK), and methyl vinyl ketone, MVK) as well as the photolysis rate constants of various trace gases were constrained to values measured during the IBAIRN campaign.

Based on the GC-AED measurements, the MTs were split into α-pinene (49 %), β-pinene (13 %), Δ-carene (27 %), and camphene (8 %). Limonene is not included in the standard chemical mechanism of CAABA/MECCA, but as its contribution to the MTs during IBAIRN was only 3 % it was treated as Δ-carene (increasing the Δ-carene contribution to 30 %).

The atmospheric methane mixing ratio was set to a constant value of 1.8 ppmv. Non-methane alkanes, the degradation of which represents $\sim$30 %–45 % of the acetaldehyde source globally (Millet et al., 2010), were constrained to 1000 pptv of ethane, 250 pptv of propane, and 150 pptv of *n*-butane, as found in similar environments in Finland (Hakola et al., 2006; Hellén et al., 2015). The mixing ratio of PAN, which is generally the most abundant of the peroxy acetyl nitrates (PNs), was calculated from a measurement of the sum of peroxy nitrates, whereby $[\mathrm{PAN}] = 0.9 \times \Sigma[\mathrm{PNs}]$ (estimation based on observations by, for example, Shepson et al., 1992b; Roberts et al., 2004; Roiger et al., 2011). The model-generated, averaged OH concentration through the diel cycle was in good agreement (within $\sim$20 %) with that calculated from the correlation of ground-level OH measurements with UVB radiation intensity at the Hyytiälä site (with $[\mathrm{OH}] = 5.62 \times 10^5\,[\mathrm{UVB}]^{0.62}$ molecule $\mathrm{cm^{-3}}$ when UVB is in units of $\mathrm{W\,m^{-2}}$; Petäjä et al., 2009; Hellén et al., 2018) but showed more variability resulting from changes in NO mixing ratios and the conversion of HO_2 to OH.

3 Results and discussion

In the following, we analyse in situ measurements of pyruvic acid to derive emission rates, present the results of the theoretical calculations of the fate of CH_3OH, and discuss the box-model output for the IBAIRN campaign with a focus on pyruvic acid emission rates and its impact on acetaldehyde and radical chemistry in the boundary layer of the boreal forest.

3.1 Pyruvic acid emission rate relative to monoterpenes during IBAIRN

In order to derive the pyruvic acid emission rate (E_{pyr}) during IBAIRN, we assume that only photolysis and dry deposition contribute significantly to its overall loss rate and that pyruvic acid is in steady state. The latter assumption is reasonable as its mean lifetime was (2 ± 0.5) h. Due to a homogeneous fetch at the measurement site, we can neglect transport processes, and E_{pyr} is defined by Eq. (1), where $[\mathrm{pyr}]_{\mathrm{ss}}$ is the measured mixing ratio, J_{pyr} is the photolysis rate constant of pyruvic acid, k_{dep} is the first-order loss rate constant for its dry deposition, and h_{MXL} is the well-mixed boundary layer height.

$$E_{\mathrm{pyr}} = [\mathrm{pyr}]_{\mathrm{ss}}(J_{\mathrm{pyr}} + k_{\mathrm{dep}})h_{\mathrm{MXL}} \tag{1}$$

E_{pyr} is effectively an emission rate normalized to the MXL height (h_{MXL}). As the photolysis is a substantial fraction of the overall losses of $CH_3C(O)C(O)OH$, the choice of quantum yield φ directly impacts the calculated emission rate.

The deposition rate of pyruvic acid was calculated from $k_{\mathrm{dep}} = v_{\mathrm{dep}} h_{\mathrm{MXL}}^{-1}$ during the day and $k_{\mathrm{dep}} = 2 v_{\mathrm{dep}} h_{\mathrm{MXL}}^{-1}$ during the night (Shepson et al., 1992a), with the transition following the diel variation in the mixing layer height h_{MXL} (see Fig. S1 in the Supplement). Further, as pyruvic acid and H_2O_2 have similar solubilities, we assumed that their deposition velocities are equal, so that $v_{\mathrm{dep}} = 8.4\,\mathrm{cm\,s^{-1}}$ during the day and $v_{\mathrm{dep}} = 0.8\,\mathrm{cm\,s^{-1}}$ during the night, as derived by Crowley et al. (2018) for the same site. This resulted in a minimum dry-deposition loss rate constant of $k_{\mathrm{dep}} = 0.9 \times 10^{-4}\,\mathrm{s^{-1}}$ during the day and a maximum of $k_{\mathrm{dep}} = 1.8 \times 10^{-4}\,\mathrm{s^{-1}}$ during the night.

The same calculation is performed for the MTs (E_{MT}) over the same period (and thus for the same MXL height). We note that h_{MXL} controls not only the value of k_{dep}, but also directly affects the mixing ratios of both MTs and pyruvic acid for a given emission rate. The relative emission rate ($E_{\mathrm{pyr}}/E_{\mathrm{MT}}$) can be calculated from Eq. (2), where terms in square brackets are concentrations.

$$\frac{E_{\mathrm{pyr}}}{E_{\mathrm{MT}}} = \frac{[\mathrm{pyr}]_{\mathrm{ss}}(J_{\mathrm{pyr}} + k_{\mathrm{dep}})}{[\mathrm{MT}]_{\mathrm{ss}}\left(k_{\mathrm{OH}}\,[\mathrm{OH}] + k_{\mathrm{NO_3}}\,[\mathrm{NO_3}] + k_{\mathrm{O_3}}\,[\mathrm{O_3}]\right)} \tag{2}$$

In the denominator, k_{OH}, $k_{\mathrm{NO_3}}$, and $k_{\mathrm{O_3}}$ are rate coefficients for reaction of MTs with OH, NO_3, and O_3, respectively. As we do not have GC data at high time resolution, an effective rate coefficient for loss of the monoterpenes was derived from the mean MT composition as measured by GC-AED (49 % α-pinene, 13 % β-pinene, 27 % carene (sum of 2-carene and 3-carene), 3 % *d*-limonene, and 8 % camphene) and the corresponding rate coefficients (Perring et al., 2013;

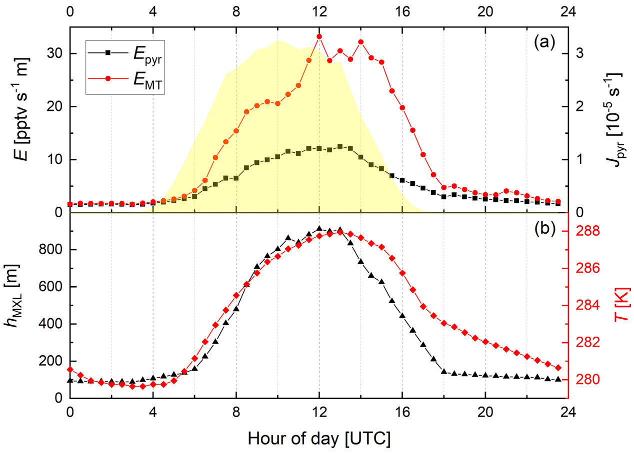

Figure 2. Diel variation of the (MXL height-corrected) emission rates of pyruvic acid (E_{pyr}, scenario B) and monoterpenes (E_{MT}) along with J_{pyr} (yellow shaded), T, and h_{MXL} for the IBAIRN campaign.

Gaona-Colman et al., 2017; IUPAC Task Group on Atmospheric Chemical Kinetic Data Evaluation, 2021). This will introduce significant uncertainty (factor of ~ 2) into the calculation of the MT emission rates. Further uncertainty arises from the measurement of pyruvic acid, ΣMT, OH, O_3, NO_3, h_{MXL}, and J_{pyr}. In particular, the results are very sensitive to the deposition velocity (v_{dep}) of pyruvic acid, which is an estimate based on the deposition velocity of H_2O_2, which itself has an uncertainty of $\sim 90\,\%$ (Fischer et al., 2019). Further, our calculations are based on the assumption that the sources of pyruvic acid and MT are evenly distributed, and measurements made at ~ 8.5 m above the ground are representative of the entire boundary layer (i.e. that the boundary layer is well-mixed, including the very shallow boundary layer at night). A gradient in pyruvic acid mixing ratios at night cannot be ruled out, which would impact on our results. We estimate that the emission ratio (E_{pyr}/E_{MT}) in Eq. (2) is associated with an overall uncertainty of a factor of ~ 3 notwithstanding the use of different quantum yields (and thus J values) for pyruvic acid photolysis.

A time series of pyruvic acid and MT mixing ratios along with the MXL height (h_{MXL}) derived from a lidar measurement and from the ERA-Interim reanalysis is shown in Fig. S2. Whereas both MXL height datasets agree very well during the night when the MXL is shallow (usually < 100 m), the lidar data are on average a factor of ~ 2 lower during the day and characterized by a much higher variability. For the derivation of the diel profile of h_{MXL} (Fig. S1), we took an average of both datasets. The diel variation displayed in Fig. S2, with the highest MT mixing ratios at night, is characteristic of this boreal forest site and has been observed in earlier studies (Hellén et al., 2018).

In the following, we focus on the mean, diel profiles of E_{pyr}, E_{MT}, J_{pyr}, T, and h_{MXL} for the IBAIRN campaign, which are presented in Fig. 2. A plot showing the variability of the MT and pyruvic acid mixing ratios over the same period was previously reported (see Fig. 3 of Eger et al., 2020).

During September, the emission rate of pyruvic acid (E_{pyr}) reaches its maximum a few hours after solar noon when the temperature peaks, similar to E_{MT}. However, the amplitude of the day-to-night difference in E_{pyr} is a factor of ~ 3 smaller than observed for E_{MT}. This could indicate that pyruvic acid emissions are less temperature-dependent than MT emissions (see below) and that other environmental factors might additionally play a role at this time of year.

The emission rates of the MTs derived as described above show a large day–night variation with values a factor of ~ 20 larger around noontime compared to midnight. This is significantly larger than the expected variation (factor of 2–3) based on the average noon-to-midnight temperature difference of 10 K and the parameterization of Guenther et al. (1993), whereby $E_{MT} \propto \exp(\beta(T - 297\,\mathrm{K}))$ with $\beta = 0.1\,\mathrm{K}^{-1}$ (which is in line in with the empirical value of $\beta = 0.12\,\mathrm{K}^{-1}$ that was derived for this site in September by Hellén et al., 2018). One potential reason for this discrepancy may be emissions in autumn from fresh leaf litter that significantly contribute to the observed mixing ratios (Hellén et al., 2018) although the assumption of evenly distributed sources and a well-mixed boundary layer is not necessarily valid during the night, especially during strong temperature inversions.

Figure S3 shows that the daytime emission of pyruvic acid relative to MT (E_{pyr}/E_{MT}) varies by a factor of ~ 2, depending on the chosen scenario, whereas the nighttime emission ratio is only dependent on the deposition velocity of pyruvic acid. For further analysis we adopt a quantum yield of 0.2, as presently preferred by IUPAC. On average, (E_{pyr}/E_{MT}) ~ 0.6, with a minimum value of ~ 0.3 in the evening and a maximum value of ~ 1 in the early morning, indicating elevated pyruvic acid emissions relative to MT at night. To derive a T-dependent expression from the diurnal profile of the emission factor, we fit an exponential function to the plot of temperature versus E_{pyr}/E_{MT} (Fig. S4), yielding

$$E_{pyr} = \left[0.28 + 3.17 \cdot \exp\left(\frac{273 - T}{4.24}\right)\right] \cdot \mathrm{EMT}. \quad (3)$$

We note that (like the values of E_{pyr}) the temperature dependence derived is strongly influenced by the diel variation of the MXL height and thus carries significant uncertainty and may not be transferable to other locations or even times of the year.

As our measurements of pyruvic acid are the first to have been made in the boreal forest, we cannot compare our relative emission ratio (E_{pyr}/E_{MT}) with previous measurements in a similar environment. Instead, where possible, we derive the emission ratio from measurements of MTs, isoprene, and pyruvic acid in warmer climates.

Jardine et al. (2010b) performed measurements in an enclosed (glass dome) tropical forest biome at Biosphere 2 in

Table 1. Emission rate of pyruvic acid ($E_{\mathbf{pyr}}$) relative to isoprene ($E_{\mathbf{iso}}$) and MT ($E_{\mathbf{MT}}$).

Reference	Location	Plant species	(E_{pyr}/E_{iso})	(E_{pyr}/E_{MT})
This study	Hyytiälä, Finland	Boreal forest	~20	0.62
Talbot et al. (1990)	Manaus, Brazil	Tropical forest	0.003	–
Jardine et al. (2010b)	Biosphere 2, Arizona, US	Tropical biome	0.17	4
Jardine et al. (2010b)	Biosphere 2, Arizona, US	Mango tree	0.05	1.7
Jardine et al. (2010a)	Biosphere 2, Arizona, US	Creosote bush	0.05	0.07

Arizona, US, where they found maximum mixing ratios of 120 ppbv isoprene, 6 ppbv MTs, and 15 ppbv pyruvic acid. As the glass dome absorbed actinic wavelengths and prevented active photochemistry, the chemical loss processes for pyruvic acid, isoprene, and MT (including photolysis and reactions with OH, O_3, and NO_3) are negligible. Initially disregarding the deposition of isoprene and MT, we derive lower limits of $(E_{pyr}/E_{iso}) \sim 0.17$ and $(E_{pyr}/E_{MT}) \sim 4$ (see Table 1). However, due to the presence of large concentrations of isoprene-consuming microbes in the soil of Biosphere 2, the isoprene loss rate via deposition may be enhanced, which will decrease the effective emission ratio (E_{pyr}/E_{iso}). In addition, branch enclosure studies were performed on a *Mangifera indica* (mango) tree within Biosphere 2, yielding mean fluxes (in $\mathrm{nmol\,m^{-2}\,s^{-1}}$) of 3.2 for isoprene, 0.09 for MT, and 0.15 for pyruvic acid. Pyruvic acid emissions peaked during the day when temperature and photosynthetically active radiation (PAR) were highest and correlated very well with isoprene emissions and (to a certain extent) with MT emissions. Assuming that a mango tree is representative of the tropical vegetation, we derive an emission ratio of $(E_{pyr}/E_{iso} \sim 0.05$ and $(E_{pyr}/E_{MT}) \sim 1.7$ (see Table 1), which is consistent with our estimations for the IBAIRN campaign. However, given that Talbot et al. (1990) observed great variability in pyruvic acid emission fluxes among five different tree species during measurements in the tropical Ducke Forest Reserve close to Manaus, Brazil, this agreement may, to some extent, be coincidental. Talbot et al. (1990) also reported a mean emission flux (derived from enclosure experiments) relative to isoprene of $(E_{pyr}/E_{iso}) \sim 0.003$, which is about 1 order of magnitude smaller than in the study of Jardine et al. (2010b). In a further branch enclosure study by Jardine et al. (2010a) emissions from a creosote bush (*Larrea divaricata*), which is typically found in US drylands, were investigated. Average noontime branch emission rates (in $\mathrm{\mu g\,C\,gdw^{-1}\,h^{-1}}$) of 7.5, 10.4, and 0.2 for isoprene, MT, and pyruvic acid resulted in relative emission ratios of $(E_{pyr}/E_{iso}) \sim 0.05$ and $(E_{pyr}/E_{MT}) \sim 0.07$ for this mixed isoprene–MT-emitting species.

The comparison with the few datasets available in the literature indicates that the variability of the emission factors (E_{pyr}/E_{MT}) and (E_{pyr}/E_{iso}) among different plant species and different environments is large. In addition, a lack of pyruvic acid measurements over different seasons in the boreal forest means that we cannot exclude that the value we derive is biased by emissions (e.g. from ground-level, decaying plant litter in September) that are particular to this season and environment. The emission rates we derive are therefore relevant for the autumnal boreal forest but require validation before being extended to other regions and seasons with confidence.

3.2 Theoretical calculations on the fate of CH_3COH

Singlet methylhydroxy carbene, CH_3COH, is best characterized as having an sp^2-hybridized central carbon, bearing an in-plane lone pair in an sp^2 orbital and an empty p orbital perpendicular to the CCO plane. The lone pairs of the hydroxy O atom back-donate into the empty p orbital, such that the most favourable geometry has the hydroxy–H atom in the CCO plane. The orientation of the terminal OH group has a large impact on the energy, with $3\,\mathrm{kcal\,mol^{-1}}$ energy difference between the *syn-* and *anti*-conformers. Due to the interaction between the hydroxy O atom and the carbene functionality, internal rotation of the OH group has a very high barrier, $24\,\mathrm{kcal\,mol^{-1}}$. Concomitantly, *syn*/*anti*-interconversion is very slow, with predicted rate coefficients at 300 K of less than $10^{-2}\,\mathrm{s^{-1}}$. Under atmospheric conditions, thermalized *syn-* and *anti*-CH_3COH are thus best considered as separate species, with possibly distinct chemistry. No information is available on the relative yield of these conformers from pyruvic acid photolysis.

3.2.1 Unimolecular reactions of CH_3COH

Both *syn-* and *anti*-CH_3COH can isomerize to vinyl alcohol over high barriers $\geq 24\,\mathrm{kcal\,mol^{-1}}$ (see Fig. 3). *Anti*-CH_3COH has an additional pathway for isomerization to acetaldehyde, with a barrier of $23\,\mathrm{kcal\,mol^{-1}}$. Due to these high barriers, the thermal rate of isomerization is comparatively slow, with a 300 K rate coefficient of $\leq 4 \times 10^{-4}\,\mathrm{s^{-1}}$ (see Table 2). As already discussed by Schreiner et al. (2011), formation of CH_3CHO from *anti*-CH_3COH is most favourable at low temperatures, owing to a thinner energy barrier and hence faster tunnelling. At temperatures above 260 K, we find that formation of $CH_2{=}CHOH$ from *anti*-CH_3COH becomes dominant, with a $\sim 3.5:1$ ratio of $CH_2{=}CHOH$ to CH_3CHO at room temperature.

Table 2. Theory-predicted high-pressure rate coefficients for reaction of singlet CH_3COH.

Reactants	Products	k(298 K)	A	n	E_a
syn-$CH_3COH + O_2$	$CH_3C(OH)OO^\bullet$	2.2×10^{-20}	5.74×10^{-22}	3.05	4092
anti-$CH_3COH + O_2$	$CH_3C(OH)OO^\bullet$	6.6×10^{-21}	1.71×10^{-22}	2.97	3960
syn-$CH_3COH + H_2O$	$CH_3CH(OH)_2$	1.9×10^{-20}	1.57×10^{-55}	13.56	−1049
anti-$CH_3COH + H_2O$	$CH_3CH(OH)_2$	5.7×10^{-21}	1.09×10^{-61}	15.61	−1443
syn-CH_3COH	*anti*-CH_3COH	8.9×10^{-3}	7.86×10^{-20}	10.77	6598
	CH_2=CHOH	1.9×10^{-4}	3.62×10^{-91}	34.20	−1444
anti-CH_3COH	*syn*-CH_3COH	2.8×10^{-5}	6.55×10^{-20}	10.71	8137
	CH_2=CHOH	9.2×10^{-5}	2.02×10^{-14}	40.40	−6660
	$CH_3C(=O)H$	3.4×10^{-4}	1.26×10^{-81}	30.96	−563
CH_2=CHOH + HCOOH	$CH_3C(=O)H$ + HCOOH	2.9×10^{-18}	1.82×10^{-76}	19.88	−6192
$CH_3C(=O)H$ + HCOOH	CH_2=CHOH + HCOOH	8.1×10^{-27}	1.09×10^{-78}	20.59	−633

Calculations were performed at the CCSD(T)//M06-2X-D3 with MC-TST level of theory. Rate coefficients are given at 298 K (s^{-1} or cm^3 $molecule^{-1}$ s^{-1}). Temperature-dependent rate coefficients can be calculated using the parameters of a Kooij expression $k(200\text{-}450\,K) = A \cdot (T/K)^n \cdot \exp(-E_a/T)$ with A given per second (s^{-1}) or cubic centimetres per molecule per second (cm^3 $molecule^{-1}$ s^{-1}) and E_a in kelvin (K).

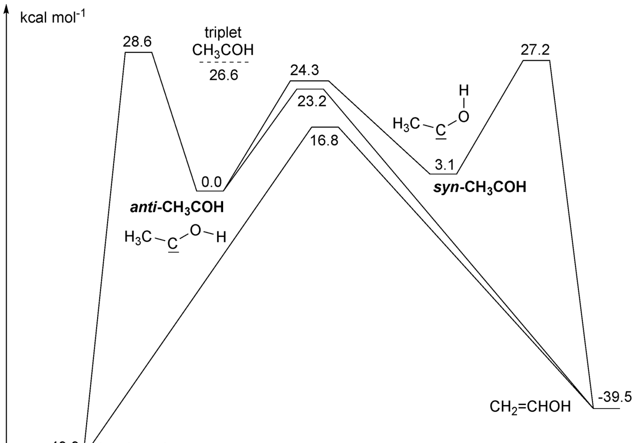

Figure 3. Zero point energy (ZPE)-corrected potential energy surface for unimolecular reactions of singlet CH_3COH at the CCSD(T)//M06-2X-D3 level of theory.

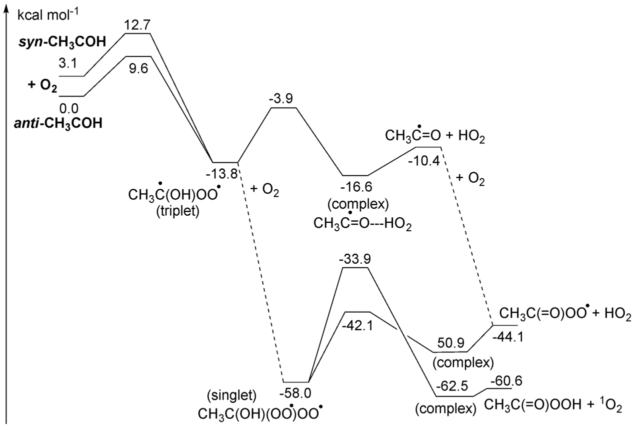

Figure 4. ZPE-corrected potential energy surface for reaction of singlet CH_3COH with O_2 at the CCSD(T)//M06-2X-D3 level of theory.

Given the low predicted thermal rate coefficients, it seems unlikely that the experimentally observed acetaldehyde and vinyl alcohol in pyruvic acid photolysis are formed from isomerization of *thermalized* CH_3COH. The energy distribution of energized, nascent carbenes would be rather broad as the available energy upon pyruvic acid photodissociation is distributed over all fragments and their relative motion, and the isomerization yield would then be pressure-dependent. The CH_3CHO and CH_2=CH_2OH isomers formed would have enough energy to undergo keto-enol tautomerization, but given the high barrier exceeding 55 kcal mol^{-1}, it is more probable they will instead be stabilized by collisional energy loss.

3.2.2 Reaction of CH_3COH with O_2

Under atmospheric conditions, the reaction with O_2 is potentially an important loss process for CH_3COH (Reed Harris et al., 2016, 2017a; Eger et al., 2020). The potential energy surface is shown in Fig. 4. Contrary to radicals, which react with O_2 by (near-)barrierless radical recombination, the singlet CH_3COH carbene does not have an unpaired electron and the reaction proceeds mostly by association of its out-of-plane empty p orbital with a lone electron pair in O_2, requiring orbital rearrangement to a triplet $C^{\bullet}OO^{\bullet}$ moiety with a sp^3-hybridized central carbon. This unfavourable process has high barriers, $> 9\,\mathrm{kcal\,mol^{-1}}$, and concomitantly low rate coefficients, $k(298\,\mathrm{K}) \sim 10^{-20}\,\mathrm{cm^3\,molecule^{-1}\,s^{-1}}$ (see Table 2). The rate coefficient is however highly uncertain, owing to an uncertainty (~ 1 to $2\,\mathrm{kcal\,mol^{-1}}$) on the barrier height.

The decomposition of the $CH_3C^{\bullet}(OH)OO^{\bullet}$ triplet diradical intermediate, forming $CH_3C^{\bullet}{=}O + HO_2$, is reminiscent of the chemistry of α-OH alkyl radicals with unpaired electrons and should occur rapidly owing to the sufficiently high energy content of the peroxyl-alkyl diradical (Hermans et al., 2005, 2004; Dillon et al., 2012; Olivella et al., 2001; Dibble, 2002). Note that this chemistry is very distinct from that of the singlet $CH_3C(OH)OO$ Criegee intermediate. The acyl radical product is expected to recombine rapidly with a second O_2 molecule, forming acylperoxy radicals, $CH_3C({=}O)OO^{\bullet}$. Alternatively, the triplet $CH_3C^{\bullet}(OH)OO^{\bullet}$ intermediate can react with a second O_2 molecule by a barrierless recombination reaction (Fig. 4), forming the diperoxy singlet diradical $CH_3C(OH)(OO^{\bullet})OO^{\bullet}$, which in turn can eliminate HO_2, similar to other α-OH peroxy radicals, forming the acylperoxy radicals directly. This second O_2 addition is sufficiently exothermic to allow for formation of peracetic acid with a singlet O_2 molecule, but this process has a rather large barrier of $\sim 24\,\mathrm{kcal\,mol^{-1}}$ and is expected to be a minor contributor, leaving $CH_3C(O)O_2 + HO_2$ as the likely dominant products of the overall reaction of CH_3COH with oxygen molecules.

3.2.3 Reactions of CH_3COH with carboxylic acids

Samanta et al. (2021) observed loss of CH_3COH via reaction with pyruvic acid, which may indicate that its fate in the atmosphere may also be (partially) controlled by similar reactions. To theoretically investigate the reaction of CH_3COH with carboxylic acids, we used formic acid in the calculations. Not only is formic acid an abundant organic acid in the atmospheric boundary layer, but also its reactivity is related to the properties of the –C(=O)OH moiety, and the results are transferable to other oxoacids, including pyruvic acid, which was present in high concentrations in most laboratory investigations.

As shown in Fig. 5, CH_3COH forms strong complexes with HC(O)OH, with $11\,\mathrm{kcal\,mol^{-1}}$ stability. From this complex, an addition process occurs that is best described as the transfer of the acidic H^+ atom to the carbene lone pair on the CH_3COH central carbon, with simultaneous association of one of the negatively charged lone electron pair of the carbonyl oxygen to the carbene vacant p orbital, forming a 1-hydroxyethyl ester ($CH_3CH(OH)OC(O)H$). Due to the concerted association of the two carbene orbitals with suitable partners in the carboxylic moiety, this process has a very low barrier ($\leq 1\,\mathrm{kcal\,mol^{-1}}$). This mechanism is feasible due to the size of the –C(O)OH group and the possibility of shifting the double bond to the other oxygen atom upon H-atom loss. For the *anti*-CH_3COH carbene, we also found that an in-plane approach of the carboxylic acid towards the COH moiety in methylhydroxy carbene can simultaneously transfer the acidic H atom to the carbene carbon while the carbene hydroxy H atom is transferred to the carbonyl oxygen in the acid, reforming the HC(O)OH co-reactant. This catalysis reaction converts *anti*-CH_3COH to acetaldehyde, CH_3CHO, without an energy barrier. Both adduct formation and the catalysis reaction should proceed with rate coefficients near the collision limit.

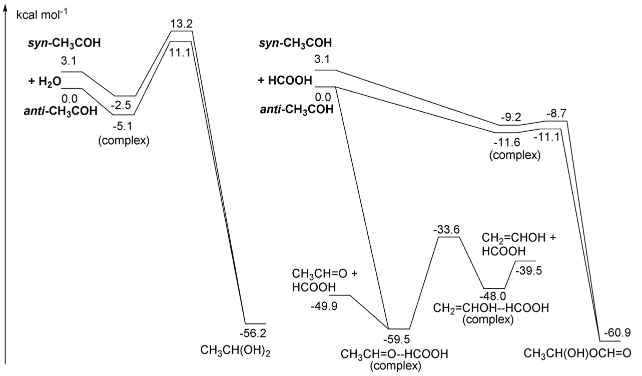

Figure 5. ZPE-corrected potential energy surface for reactions of singlet CH_3COH with H_2O (left) and HCOOH (right) at the CCSD(T)//M06-2X-D3 level of theory.

Carboxylic acids can also catalyse keto-enol tautomerization, possibly helping the isomerization between CH_3CHO and $CH_2{=}CH_2OH$ by reducing the effective barrier by over $50\,\mathrm{kcal\,mol^{-1}}$ though the thermal reaction remains slow (see Table 2). The only reaction of CH_3COH that has been investigated experimentally to date is that with pyruvic acid (Samanta et al., 2021), which we also examine theoretically in the Supplement. Note that the large rate coefficient for CH_3COH with organic acids calculated here would imply that reaction of *thermalized* CH_3COH with pyruvic acid would overwhelm any other bimolecular CH_3COH reaction in their work and most of the experiments listed in Table S1.

3.2.4 Reactions of CH_3COH with H_2O

Based on the reactivity of small carbenes towards closed-shell molecules, Samanta et al. (2021) suggested that reaction with H_2O might be an important loss process of the CH_3COH carbene intermediate. We have characterized the insertion reaction of CH_3COH in the H_2O molecule and found very high barriers, $\geq 11\,\mathrm{kcal\,mol^{-1}}$, with very low rate coefficients $\sim 10^{-20}\,\mathrm{cm^3\,molecule^{-1}\,s^{-1}}$ (see Fig. 5 and Table 2). The reaction is significantly slower than with carboxylic acid as the smaller H_2O molecule is unable to simultaneously reach both carbene orbitals in a favourable geometry. The reaction of H_2O with CH_3COH is best described as a shift of an H^+ atom to the carbene lone pair orbital, followed by migration of the water HO^- moiety to the vacant carbene orbital to form a bond with a lone electron pair. The reaction is further hindered by the back-donation of the CH_3COH oxygen atom into the vacant carbene orbital, partially filling the vacant carbene orbital and reducing the reactivity of the carbene functionality. We therefore propose that CH_3COH will be significantly less reactive towards closed shell species than the ^2CH and $^1CH_2$ carbenes which are known to exhibit very fast insertion and cyclo-addition reactions (Vereecken et al., 1998; Goulay et al., 2009; Douglas et al., 2019; Jasper et al., 2007; Gannon et al., 2010).

3.2.5 Summary of theoretical calculations: the fate of thermalized CH_3COH in 1 bar of air

The theoretical analysis of the fate of CH_3COH carbene intermediates formed in PA photolysis indicates that the acetaldehyde formation observed in many experiments could be the result of a fast catalysis reaction of CH_3COH with pyruvic acid, which under typical experimental conditions dominates over competing reactions, such as with O_2, by several orders of magnitude. This conclusion is consistent with the experimental observations of Reed Harris et al. (2017a), who report a reduction in the acetaldehyde yield when low pyruvic acid concentrations are used and an increase in the formation of acetic acid (which can be formed in the reaction of $CH_3C(O)O_2$ radicals with HO_2). In the atmospheric boundary layer atmosphere, where the concentrations of organic acids may lie between 10^{10} and 10^{11} molecule cm^{-3} (Millet et al., 2015) and that of O_2 is close to 5×10^{18} molecule cm^{-3}, the reactions of CH_3COH with organic acids and O_2 are competitive, whereas reaction of CH_3COH with water is minor. Table 2 lists the predicted rate coefficients for these reactions.

3.3 Box-model results: contribution of pyruvic acid to acetaldehyde and radical formation

To account for the large variability in photodissociation quantum yields and product yields reported in the literature (see above), we modelled two scenarios, A and B:

- *Scenario A*. In this scenario we used pyruvic acid cross sections, quantum yields, and product yields according to the IUPAC recommendations with a photodissociation quantum yield (φ) of 0.2 at 1 bar pressure and branching ratios of 0.6, 0.05, and 0.35 for Reactions (R1), (R2), and (R3) as listed in Sect. 1.1.
- *Scenario B*. Here we use the same absorption cross-sections as scenario A but build on the recent observations of (Samanta et al., 2021) and the theoretical work presented in Sect. 3.2, which considers the formation and fate of an excited CH_3COH molecule ($+CO_2$). In scenario B, we consider the effects of using photodissociation quantum yields of 0.2, 0.5, and 1 (scenarios $B_{0.2}$, $B_{0.5}$, and B_1, respectively). Photolysis at wavelengths < 340 nm was considered to generate $CH_3CO + HOCO$, whereas photolysis at wavelengths > 340 nm was assumed to form CO_2 + energy rich $CH_3COH^\#$, which undergoes the reactions outlined in Sect. 1. Assuming a quantum yield that is independent of wavelength results in 25 % of pyruvic acid photolysis at noon taking place at wavelengths < 340 nm and 75 % at wavelengths > 340 nm. In the model, we assume that this ratio does not change (i.e. we neglect wavelength-dependent variations in the relative actinic flux through the diel cycle). The values of 25 % and 75 % listed above roughly correspond to the relative importance of peroxy radical formation (via Reactions R3, R4, and R5) at the shorter wavelengths compared to $CH_3COH + CO_2$ formation (Reaction R6) at the longer wavelengths. Some experimental data indicate that addition of O_2 can reduce the CH_3CHO yield in favour of formation of, for example, acetic acid. For this reason we use a rate coefficient for reaction of CH_3COH with O_2 that is competitive with the reaction between CH_3COH and organic acids. This is a factor of ~ 10 larger than the value obtained theoretically, but we consider this value still within the uncertainty (~ 1 to 2 kcal mol^{-1} on the barrier height) of our current theoretical results as the peculiar wavefunction of CH_3COH may require even higher levels of theory to be described accurately.

In the box model, in addition to reaction with O_2, the thermalized carbene also reacts with formic and acetic acids to form acetaldehyde:

$$CH_3COH + HCOOH \rightarrow CH_3CHO + HCOOH \quad (R12)$$

$$CH_3COH + CH_3C(O)OH \rightarrow CH_3CHO + CH_3C(O)OH \quad (R13)$$

with a rate coefficient of 5×10^{-11} cm^3 $molecule^{-1}$ s^{-1}.

We assumed that (at 1 bar) 70 % of $CH_3COH^\#$ was quenched to CH_3COH, 20 % isomerized to CH_3CHO, and 10 % isomerized to $CH_2{=}CHOH$ in order to reproduce the CH_3CHO-to-$CH_2{=}CHOH$ ratio reported by Samanta et al. (2021). A summary reaction scheme for the photodissociation of pyruvic acid and the fate of the initial products is given in the SI.

3.3.1 CH_3CHO formation

The modelled formation of CH_3CHO from pyruvic acid photolysis through the diel cycle when considering scenario A is displayed as a stacked plot of contributing reactions in Fig. 6. Immediately apparent from this figure is the dominance of pyruvic acid photolysis compared to all other processes. Under scenario A, even with the low quantum yield ($\varphi = 0.2$) recommended by IUPAC, pyruvic acid photolysis contributes > 80 % to the overall CH_3CHO production term, with a maximum of ~ 15 % (at noon) arising from reactions

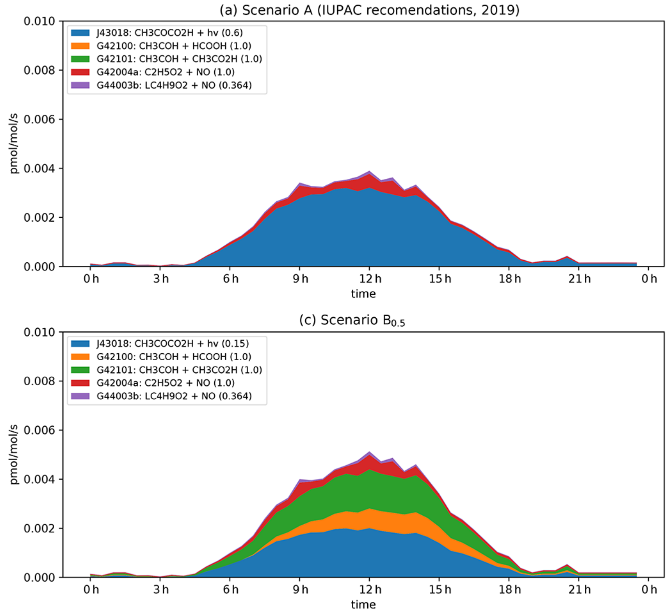

Figure 6. Modelled rates of CH_3CHO formation (in pptv s^{-1}) through the diel cycle from photolysis of pyruvic acid (blue, orange, and green) and other reactions during IBAIRN. **(a)** Scenario A (IUPAC). **(b)** Scenario B_1. **(c)** Scenario $B_{0.5}$. **(d)** Scenario $B_{0.2}$. In the legend, the first term is the equation tag used by CAABA/MECCA for the reaction. LC4H9O2 is the peroxy radical formed in the reaction of OH with butane. A full listing of the reactions can be downloaded (see Data availability section).

of the ethylperoxy radical, formed in the reaction of OH with ethane (7.5 %) and butane (3.75 %) and in the photolysis of $CH_3C(O)C_2H_5$ (3.75 %).

Under scenario B, pyruvic acid photolysis still dominates the formation of CH_3CHO, with a noontime contribution of 91 %, 86 %, and 71 % when quantum yields of 1, 0.5, and 0.2 are considered. Of the pyruvic acid contribution, 45 % of the CH_3CHO arises via isomerization of the initially formed, energized carbene (blue), while the remaining 55 % results from reactions of the thermalized carbene with formic (orange) and acetic (green) acids, the concentrations of which were constrained by observations. The modelled, noontime mixing ratio of CH_3CHO varies from 400 pptv (scenario B_1) to 160 pptv (scenario $B_{0.2}$) when pyruvic acid photolysis is included and is reduced to ~ 100 pptv when the quantum yield is set to zero. Unfortunately, reliable measurements of the CH_3CHO mixing ratios with which to compare the model simulations were not available for the IBAIRN campaign as the in situ PTR-MS data set ($m/z45$) varied from -400 to $+400$ pptv over the diel cycle. The modelled, maximum mixing ratio of CH_3CHO increases from ~ 100 pptv when pyruvic acid photolysis is neglected to > 400 pptv under scenario B_1 (see Fig. S6).

3.3.2 $CH_3C(O)O_2$ formation

The $CH_3C(O)O_2$ radical is formed in a termolecular reaction between the CH_3CO radical and O_2. Figure 7 displays the main photochemical reactions that lead to the formation of CH_3CO in our model. The spikes in the simulated production rates are connected to spikes in the diel average NO mixing ratio at the site. In analysing the data, we therefore consider not only the contributions at noon (when NO mixing ratios were large), but also at 10:30 when NO mixing ratios were comparably low.

Under scenario A, where $\varphi = 0.2$ and the yield of the CH_3CO radical is 0.35, the contribution of pyruvic acid photolysis to the overall production rate at 12:00 and 10:30 is about 23 % and 16 %, respectively, roughly equally divided into a direct contribution (J43018) and an indirect contribution (G42008a) arising via enhanced CH_3CHO levels. The main contributors to the formation of CH_3CO are reactions initiated by the degradation of isoprene and MTs (in the legend of Fig. 7: BIACETO2, C511O2, C716O2, CO23C4CHO, CO235C6CHO), which involve reactions of peroxy radicals with NO.

Under scenario B_1, the photolysis of pyruvic acid becomes significantly more important, contributing a total of 63 % of the total production rate for CH_3CO at 10:30 and 42 % at 12:00. When considering scenarios $B_{0.5}$ and $B_{0.2}$ the contributions of pyruvic acid photolysis are reduced to 46 % (29 %) and 29 % (17 %), respectively, where the numbers in parentheses are for the "high-NO_x" situation. Generally, the reaction of the thermalized carbene with O_2 (G42099), the direct photolysis at wavelengths < 340 nm (J43018), and the indirect enhancement in CH_3CO formation via the enhanced levels of CH_3CHO (G42008a) contribute roughly equally to the formation of CH_3CO resulting from pyruvic acid photol-

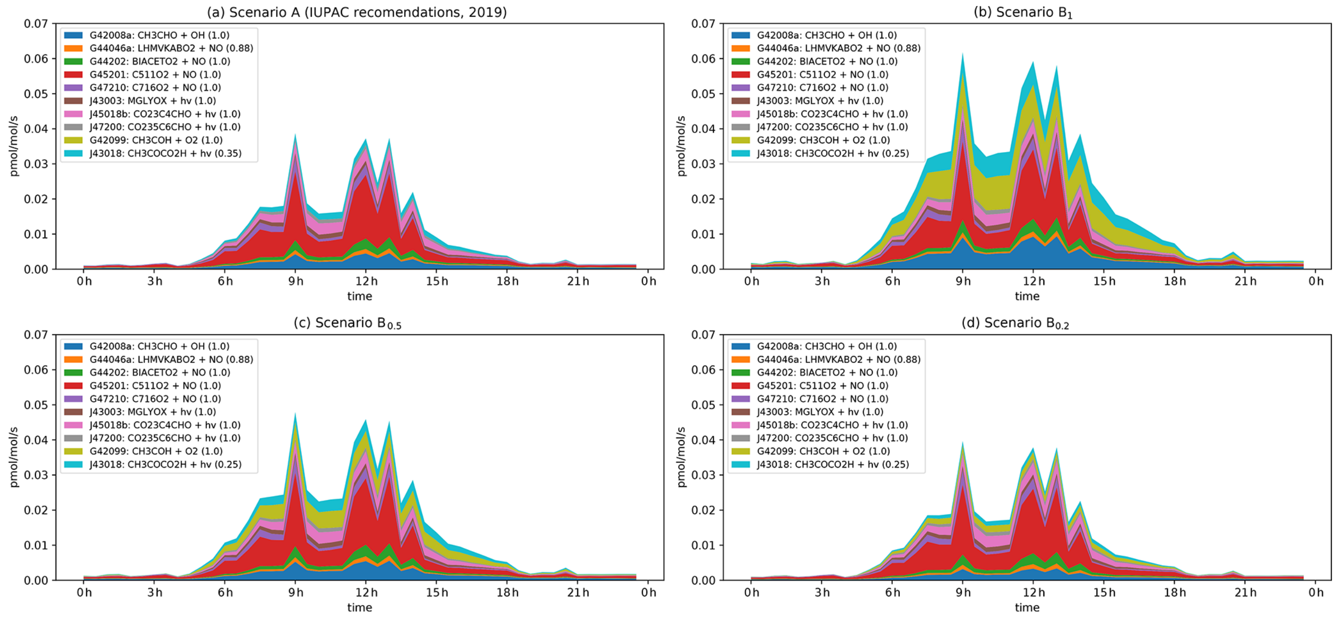

Figure 7. Modelled rates of CH_3CO formation (in pptv s^{-1}) through the diel cycle from photolysis of pyruvic acid (blue, orange, and green) and other photochemical processes during IBAIRN. **(a)** Scenario A (IUPAC). **(b)** Scenario B_1. **(c)** Scenario $B_{0.5}$. **(c)** Scenario $B_{0.2}$. In the legend, the first term is the equation tag used by CAABA/MECCA for the reaction. A full listing of the reactions can be downloaded (see Data availability section).

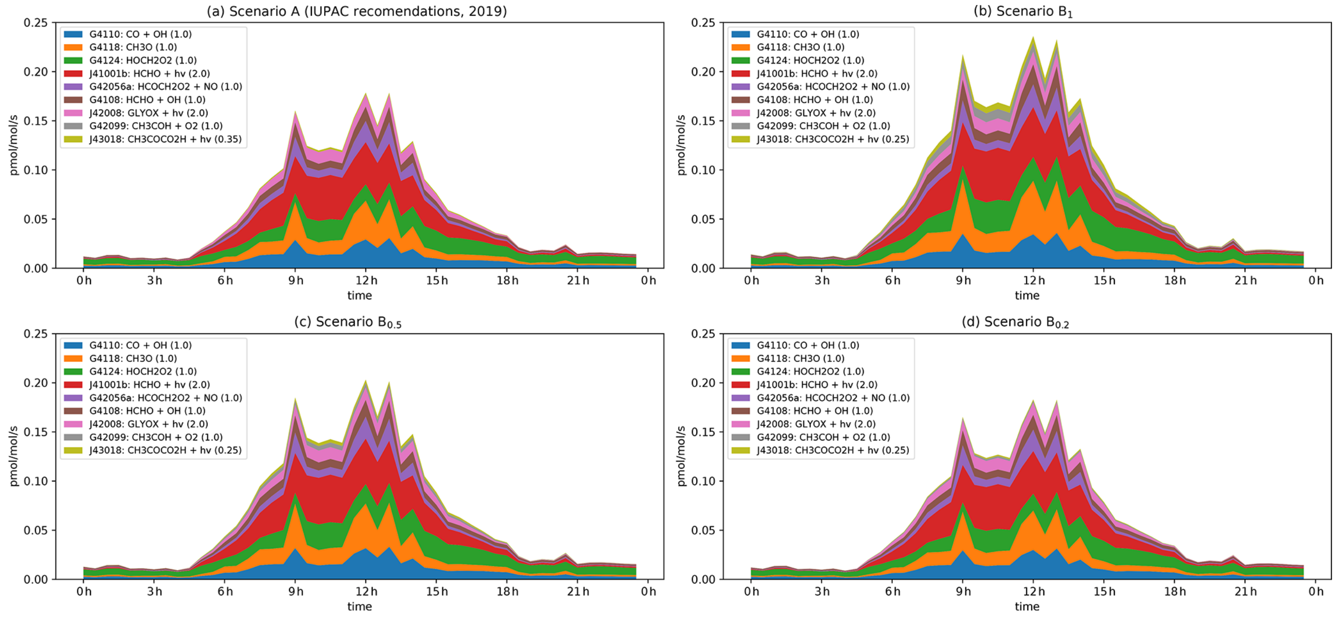

Figure 8. Modelled rates of HO_2 formation (in pptv s^{-1}) through the diel cycle from photolysis of pyruvic acid (blue, orange, and green) and other photochemical processes during IBAIRN. **(a)** Scenario A (IUPAC). **(b)** Scenario B_1. **(c)** Scenario $B_{0.5}$. **(d)** Scenario $B_{0.2}$. In the legend, the first term is the MCM designation for the reaction. A full listing of the reactions can be downloaded (see Data availability section).

ysis. The modelled mixing ratio of the $CH_3C(O)O_2$ radical at noon increases by a factor of ~ 1.5 when comparing scenario B_1 with the quantum yields for pyruvic acid photodissociation set to zero.

3.3.3 HO_2 formation

In Fig. 8, we plot the nine most important model pathways to HO_2 production through the diel cycle. The dominant modelled production terms for HO_2 involve HCHO (photolysis HCHO and reaction with OH, G4108, J41001b), the reaction of methoxy radicals (G4118, whereby CH_3O is generated mainly in the reaction of CH_3O_2 radicals with NO), and the reaction of OH with CO. The direct contribution of pyruvic acid photolysis to HO_2 formation (via its photolysis (J43018) and through the reaction of CH_3COH with O_2, G42099) is $\sim 10\,\%$ under scenario B_1 under low-NO_x conditions (i.e. at 10:30). Under all other scenarios it is lower, with values (in percent) of < 1 (scenario A at both 10:30 and 02:00), ~ 6 (scenario B_1 at 12:00), ~ 5 and ~ 3.5 (scenario $B_{0.5}$ at 10:30 and 12:00, respectively), and ~ 1.5 and < 1 (scenario $B_{0.2}$ at 10:30 and 12:00, respectively). However, although the direct impact of pyruvic acid photolysis is weak, it has a significant indirect effect via the enhanced formation of $CH_3C(O)O_2$ radicals (directly via Reactions R3 + R4 and R10 and indirectly via CH_3CHO formation), which, in the presence of O_2, reacts with NO to form CH_3O_2. Enhanced production rates of CH_3O_2 result in enhanced production rates of CH_3O and HCHO and thus HO_2.

$$CH_3C(O)O_2 + NO(+O_2) \rightarrow CH_3O_2 + NO_2 + CO_2 \quad \text{(R14)}$$

$$CH_3O_2 + NO \rightarrow CH_3O + NO_2 \quad \text{(R15)}$$

$$CH_3O + O_2 \rightarrow HCHO + HO_2 \quad \text{(R16)}$$

$$HCHO + h\nu(+2O_2) \rightarrow 2HO_2 + CO \quad \text{(R17)}$$

The model simulations have shown that the photolysis of pyruvic acid at the levels observed during the IBAIRN campaign has a potentially significant effect on both CH_3CHO mixing ratios and production rates of HO_2 and $CH_3C(O)O_2$ radicals, the latter being especially enhanced under low-NO_x conditions. The enhanced production rates and concentrations of $CH_3C(O)O_2$ and HO_2 also result in significant increases in the modelled mixing ratios of several trace gases that are formed from these radicals. Comparing scenario B_1 to the case in which the pyruvic acid photodissociation quantum yield (φ) is set to zero results in an increase by factors of 2.2, 2.0, and 1.6 for $CH_3C(O)OOH$, CH_3OOH, and H_2O_2, respectively (see Fig. S6). HCHO mixing ratios are enhanced by a factor of 1.2. Vinyl alcohol mixing ratios of up to 40 pptv were generated in scenario B_1. Clearly, the photolysis of pyruvic acid can potentially impact strongly on the concentrations of, for example, C1 and C2 carbonyl compounds and peroxides in the boreal environment.

4 Conclusions

We have combined measurements of pyruvic acid in an autumn campaign in the boreal forest (IBAIRN) with theoretical calculations designed to characterize the fate of the methylhydroxy carbene radical (CH_3COH, the major product of pyruvic acid photodissociation) with a box-modelling study. We investigated the impact of pyruvic acid photolysis on the rates of production of acetaldehyde (CH_3CHO) and the peroxy radicals $CH_3C(O)O_2$ and HO_2. The theoretical study revealed unexpected features of CH_3COH chemistry, including slow reactions of thermalized carbene with H_2O but an efficient acid-catalysed conversion to CH_3CHO in the presence of organic acids such as HC(O)OH. The reaction of CH_3COH with O_2 is slow but will contribute to its fate (and thus the formation of $CH_3C(O)O_2$ and HO_2) in the lower atmosphere where O_2 concentrations are high if the rate constant used (elevated by an order of magnitude compared to the theoretical value) is correct.

In our box model, the photolysis of pyruvic acid was parameterized as presently recommended by IUPAC (whereby the main products are CH_3CHO and CO_2) and also using a more detailed mechanism in which the formation and fate of CH_3COH was considered and in which the quantum yield was varied. In all scenarios, we find that the photolysis of pyruvic acid was the dominant source of CH_3CHO during IBAIRN and that its instantaneous contribution to the daytime formation of $CH_3C(O)O_2$ varied between 16 % and 63 %, dependent on the assumed scenario and also on the NO concentration. Pyruvic acid photodissociation results in a significant increase in the mixing ratios of several carbonyl compounds and peroxides in the boreal environment.

The results of our modelling study are strongly dependent on the chosen quantum yields and photodissociation mechanism. To reduce the uncertainty in the role of pyruvic acid photolysis, there is an urgent need for further experimental and theoretical work on the photochemistry of pyruvic acid and on the fate of methylhydroxy carbene under atmospheric conditions. In addition, further measurements of pyruvic acid mixing ratios and of its deposition velocity in different environments are required to better constrain its abundance and lifetime and thus the impact of its photolysis. Enclosure studies would be helpful to investigate the dependence of pyruvic acid emission rates on different plant types and environmental conditions.

Data availability. The Max Planck Institute data used for the IBAIRN analysis and the reaction scheme used in the box model are archived at https://doi.org/10.5281/zenodo.3254828 (Crowley and Fischer, 2019).

Supplement. The supplement related to this article is available online at: https://doi.org/10.5194/acp-21-14333-2021-supplement.

Author contributions. PGE was responsible for the pyruvic acid measurement during IBAIRN. PGE and JNC, with contributions from JL, wrote the manuscript. LV conducted the theoretical calculation on the fate of methylhydroxy carbene, RS and AP did the box modelling, and NS was responsible for the CRDS measurements of NO_2 and PANs during IBAIRN. JS was responsible for the O_3 and J value measurements during IBAIRN. HF was responsible for the NO and CO measurements during IBAIRN. EK and JW were responsible for the MT measurements during IBAIRN. VV was responsible for the mixing layer height measurements during IBAIRN. TP was responsible for the SMEAR II observations and infrastructure. All authors contributed to the paper.

Competing interests. The authors declare that they have no conflict of interest.

Acknowledgements. We thank the technical staff of SMEAR II station for the excellent support during IBAIRN.

Financial support. This research has been supported by the ENVRIplus (grant no. 654182). We are grateful to ENVRIplus for partial financial support of the IBAIRN campaign.

The article processing charges for this open-access publication were covered by the Max Planck Society.

Review statement. This paper was edited by Gabriele Stiller and reviewed by two anonymous referees.

References

Aalto, J., Porcar-Castell, A., Atherton, J., Kolari, P., Pohja, T., Hari, P., Nikinmaa, E., Petaja, T., and Back, J.: Onset of photosynthesis in spring speeds up monoterpene synthesis and leads to emission bursts, Plant Cell Environ., 38, 2299–2312, https://doi.org/10.1111/pce.12550, 2015.

Alecu, I. M., Zheng, J. J., Zhao, Y., and Truhlar, D. G.: Computational thermochemistry: scale factor databases and scale factors for vibrational frequencies obtained from electronic model chemistries, J. Chem. Theor. Comput., 6, 2872–2887, https://doi.org/10.1021/ct100326h, 2010.

Andreae, M. O., Talbot, R. W., and Li, S. M.: Atmospheric measurements of pyruvic and formic acid, J. Geophys. Res.-Atmos., 92, 6635–6641, https://doi.org/10.1029/JD092iD06p06635, 1987.

Berges, M. G. M. and Warneck, P.: Product quantum yields for the 350 nm photodecomposition of pyruvic-acid in air, Ber. Bunsen Phys. Chem., 96, 413–416, https://doi.org/10.1002/bbpc.19920960334, 1992.

Burkholder, J. B., Sander, S. P., Abbatt, J., Barker, J. R., Huie, R. E., Kolb, C. E., Kurylo, M. J., Orkin, V. L., Wilmouth, D. M., and Wine, P. H.: Chemical Kinetics and Photochemical Data for Use in Atmospheric Studies, Evaluation No. 18, JPL Publication 15-10, Jet Propulsion Laboratory, Pasadena, available at: http://jpldataeval.jpl.nasa.gov (last access: September 2020), 2015.

Calvert, J. G., Mellouki, A., Pilling, M. J., and Wallington, T. J.: The Mechanisms of Atmospheric Oxidation of the Oxygenates, Oxford Univ. Press, New York, 2011.

Chang, X.-P., Fang, Q., and Cui, G.: Mechanistic photodecarboxylation of pyruvic acid: Excited-state proton transfer and three-state intersection, J. Chem. Phys., 141, 154311, https://doi.org/10.1063/1.4898085, 2014.

Crowley, J. N. and Fischer, H.: IBAIRN data (Boreal forest, Hyytiälä Sept. 2016) Max-Planck-Institut, Mainz [data set], Zenodo, https://doi.org/10.5281/zenodo.3254828, 2019.

Crowley, J. N., Pouvesle, N., Phillips, G. J., Axinte, R., Fischer, H., Petäjä, T., Nölscher, A., Williams, J., Hens, K., Harder, H., Martinez-Harder, M., Novelli, A., Kubistin, D., Bohn, B., and Lelieveld, J.: Insights into HO_x and RO_x chemistry in the boreal forest via measurement of peroxyacetic acid, peroxyacetic nitric anhydride (PAN) and hydrogen peroxide, Atmos. Chem. Phys., 18, 13457–13479, https://doi.org/10.5194/acp-18-13457-2018, 2018.

Dee, D. P., Uppala, S. M., Simmons, A. J., Berrisford, P., Poli, P., Kobayashi, S., Andrae, U., Balmaseda, M. A., Balsamo, G., Bauer, P., Bechtold, P., Beljaars, A. C. M., van de Berg, L., Bidlot, J., Bormann, N., Delsol, C., Dragani, R., Fuentes, M., Geer, A. J., Haimberger, L., Healy, S. B., Hersbach, H., Hólm, E. V., Isaksen, L., Kållberg, P., Köhler, M., Matricardi, M., McNally, A. P., Monge-Sanz, B. M., Morcrette, J.-J., Park, B.-K., Peubey, C., de Rosnay, P., Tavolato, C., Thépaut, J.-N., and Vitart, F.: The ERA-Interim reanalysis: configuration and performance of the data assimilation system, Q. J. Roy. Meteorol. Soc., 137, 553–597, https://doi.org/10.1002/qj.828, 2011.

Dibble, T. S.: Mechanism and dynamics of the $CH_2OH + O_2$ reaction, Chem. Phys. Lett., 355, 193–200, https://doi.org/10.1016/S0009-2614(02)00211-7, 2002.

Dillon, T. J., Pozzer, A., Vereecken, L., Crowley, J. N., and Lelieveld, J.: Does acetone react with HO_2 in the upper-troposphere?, Atmos. Chem. Phys., 12, 1339–1351, https://doi.org/10.5194/acp-12-1339-2012, 2012.

Douglas, K. M., Blitz, M. A., Feng, W. H., Heard, D. E., Plane, J. M. C., Rashid, H., and Seakins, P. W.: Low temperature studies of the rate coefficients and branching ratios of reactive loss vs quenching for the reactions of (CH_2)-C-1 with C_2H_6, C_2H_4, C_2H_2, Icarus, 321, 752–766, https://doi.org/10.1016/j.icarus.2018.12.027, 2019.

Dunning, T. H.: Gaussian-basis sets for use in correlated molecular calculations. 1. the atoms boron through neon and hydrogen, J. Chem. Phys., 90, 1007–1023, https://doi.org/10.1063/1.456153, 1989.

Eckart, C.: The penetration of a potential barrier by electrons, Phys. Rev., 35, 1303–1309, https://doi.org/10.1103/PhysRev.35.1303, 1930.

Eger, P. G., Schuladen, J., Sobanski, N., Fischer, H., Karu, E., Williams, J., Riva, M., Zha, Q., Ehn, M., Quéléver, L. L. J., Schallhart, S., Lelieveld, J., and Crowley, J. N.: Pyruvic acid in the boreal forest: gas-phase mixing ratios and impact on radical chemistry, Atmos. Chem. Phys., 20, 3697–3711, https://doi.org/10.5194/acp-20-3697-2020, 2020.

Eugene, A. J., Pillar, E. A., Colussi, A. J., and Guzman, M. I.: Enhanced Acidity of Acetic and Pyruvic Acids on the Surface of Water, Langmuir, 34, 9307–9313, https://doi.org/10.1021/acs.langmuir.8b01606, 2018.

Fischer, H., Axinte, R., Bozem, H., Crowley, J. N., Ernest, C., Gilge, S., Hafermann, S., Harder, H., Hens, K., Janssen, R. H. H., Königstedt, R., Kubistin, D., Mallik, C., Martinez, M., Novelli, A., Parchatka, U., Plass-Dülmer, C., Pozzer, A., Regelin, E., Reiffs, A., Schmidt, T., Schuladen, J., and Lelieveld, J.: Diurnal variability, photochemical production and loss processes of hydrogen peroxide in the boundary layer over Europe, Atmos. Chem. Phys., 19, 11953–11968, https://doi.org/10.5194/acp-19-11953-2019, 2019.

Fischer, L., Breitenlechner, M., Canaval, E., Scholz, W., Striednig, M., Graus, M., Karl, T. G., Petäjä, T., Kulmala, M., and Hansel, A.: First Eddy Covariance Flux Measurements of Semi Volatile Organic Compounds with the PTR3-TOF-MS, Atmos. Meas. Tech. Discuss. [preprint], https://doi.org/10.5194/amt-2021-117, in review, 2021.

Frisch, M. J., Trucks, G. W., Schlegel, H. B., Scuseria, G. E., Robb, M. A., Cheeseman, J. R., Scalmani, G., Barone, V., Mennucci, B., Petersson, G. A., Nakatsuji, H., Li, X., Caricato, M., Marenich, A. V., Bloino, J., Janesko, B. G., Gomperts, R., Mennucci, B., Hratchian, H. P., Ortiz, J. V., Izmaylov, A. F., Sonnenberg, J. L., Williams-Young, D., Ding, F., Lipparini, F., Egidi, F., Goings, J., Peng, B., Petrone, A., Henderson, T., Ranasinghe, D., Zakrzewski, V. G., Gao, J., Rega, N., Zheng, G., Liang, W., Hada, M., Eara, M., Toyota, K., Fukuda, R., Hasegawa, J., Ishida, M., Nakajima, T., Honda, Y., Kitao, O., Nakai, H., Vreven, T., Throssell, K., Mntgomery, Jr., J. A., Peralta, J. E., Ogliaro, F., Bearpark, M. J., Heyd, J. J., Brothers, E. N., Kudin, K. N., Staroverov, V. N., Keith, T. A., Kobayashi, R., Normand, J., Raghavachari, K., Rendell, A. P., Burant, J. C., Iyengar, S. S., Tomasi, J., Cossi, M., Millam, J. M., Klene, M., Adamo, C., Cammi, R., Ochterski, J. W., Martin, R. L., Morokuma, K., Farkas, O., Foresman, J. B., and Fox, D. J.: Gaussian 16, Revision B.01, Gaussian Inc., Wallington, CT, 2016.

Gannon, K. L., Blitz, M. A., Liang, C. H., Pilling, M. J., Seakins, P. W., and Glowacki, D. R.: Temperature Dependent Kinetics (195–798 K) and H Atom Yields (298–498 K) from Reactions of (CH_2)-C-1 with Acetylene, Ethene, and Propene, J. Phys. Chem. A, 114, 9413–9424, https://doi.org/10.1021/jp102276j, 2010.

Gaona-Colman, E., Blanco, M. B., Barnes, I., Wiesen, P., and Teruel, M. A.: OH- and O-3-initiated atmospheric degradation of camphene: temperature dependent rate coefficients, product yields and mechanisms, RSC Adv., 7, 2733–2744, https://doi.org/10.1039/c6ra26656h, 2017.

Goulay, F., Trevitt, A. J., Meloni, G., Selby, T. M., Osborn, D. L., Taatjes, C. A., Vereecken, L., and Leone, S. R.: Cyclic Versus Linear Isomers Produced by Reaction of the Methylidyne Radical (CH) with Small Unsaturated Hydrocarbons, J. Am. Chem. Soc., 131, 993–1005, https://doi.org/10.1021/ja804200v, 2009.

Grimme, S., Ehrlich, S., and Goerigk, L.: Effect of the Damping Function in Dispersion Corrected Density Functional Theory, J. Comput. Chem., 32, 1456–1465, https://doi.org/10.1002/jcc.21759, 2011.

Grosjean, D.: Atmospheric reactions of pyruvic acid, Atmos. Environ., 17, 2379–2382, https://doi.org/10.1016/0004-6981(83)90242-1, 1983.

Grosjean, D.: Atmospheric reactions of ortho cresol: gas phase and aerosol products, Atmos. Environ., 18, 1641–1652, https://doi.org/10.1016/0004-6981(84)90386-X, 1984.

Grosjean, D., Williams, E. L., and Grosjean, E.: Atmospheric chemistry of isoprene and of its carbonyl products, Environ. Sci. Technol., 27, 830–840, https://doi.org/10.1021/es00042a004, 1993.

Guenther, A. B., Zimmerman, P. R., Harley, P. C., Monson, R. K., and Fall, R.: Isoprene and monoterpene emission rate variability - model evaluations and sensitivity analyses, J. Geophys. Res.-Atmos., 98, 12609–12617, https://doi.org/10.1029/93jd00527, 1993.

Hakola, H., Hellén, H., and Laurila, T.: Ten years of light hydrocarbons (C_2–C_6) concentration measurements in background air in Finland, Atmos. Environ., 40, 3621–3630, https://doi.org/10.1016/j.atmosenv.2005.08.019, 2006.

Hallquist, M., Wenger, J. C., Baltensperger, U., Rudich, Y., Simpson, D., Claeys, M., Dommen, J., Donahue, N. M., George, C., Goldstein, A. H., Hamilton, J. F., Herrmann, H., Hoffmann, T., Iinuma, Y., Jang, M., Jenkin, M. E., Jimenez, J. L., Kiendler-Scharr, A., Maenhaut, W., McFiggans, G., Mentel, Th. F., Monod, A., Prévôt, A. S. H., Seinfeld, J. H., Surratt, J. D., Szmigielski, R., and Wildt, J.: The formation, properties and impact of secondary organic aerosol: current and emerging issues, Atmos. Chem. Phys., 9, 5155–5236, https://doi.org/10.5194/acp-9-5155-2009, 2009.

Hari, P. and Kulmala, M.: Station for Measuring Ecosystem–Atmosphere Relations (SMEAR II), Boreal Environ. Res., 10, 315–322, https://doi.org/10.1007/978-94-007-5603-8_9, 2005.

Helas, G., Bingemer, H., and Andreae, M. O.: Organic acids over equatorial Africa: Results from DECAFE 88, J. Geophys. Res.-Atmos., 97, 6187–6193, https://doi.org/10.1029/91jd01438, 1992.

Hellén, H., Kouznetsov, R., Anttila, P., and Hakola, H.: Increasing influence of easterly air masses on NMHC concentrations at the Pallas-Sodankylä GAW station, Boreal Environ. Res., 20, 542–552, 2015.

Hellén, H., Praplan, A. P., Tykkä, T., Ylivinkka, I., Vakkari, V., Bäck, J., Petäjä, T., Kulmala, M., and Hakola, H.: Long-term measurements of volatile organic compounds highlight the importance of sesquiterpenes for the atmospheric chemistry of a boreal forest, Atmos. Chem. Phys., 18, 13839–13863, https://doi.org/10.5194/acp-18-13839-2018, 2018.

Hermans, I., Nguyen, T. L., Jacobs, P. A., and Peeters, J.: Tropopause chemistry revisited: HO_2-initiated oxidation as an efficient acetone sink, J. Am. Chem. Soc., 126, 9908–9909, https://doi.org/10.1021/ja0467317, 2004.

Hermans, I., Muller, J. F., Nguyen, T. L., Jacobs, P. A., and Peeters, J.: Kinetics of alpha-hydroxy-alkylperoxyl radicals in oxidation processes. HO_2 center dot-initiated oxidation of ketones/aldehydes near the tropopause, J. Phys. Chem. A, 109, 4303–4311, 2005.

IUPAC Task Group on Atmospheric Chemical Kinetic Data Evaluation (Ammann, M., Cox, R. A., Crowley, J. N., Herrmann, H., Jenkin, M. E., McNeill, V. F., Mellouki, A., Rossi, M. J., Troe, J., and Wallington, T. J.): Evaluated kinetic and photochemical data for atmospheric chemistry, available at: http://iupac.pole-ether.fr/index.html, last access: June 2021.

Jacob, D. J. and Wofsy, S. C.: Photochemistry of biogenic emissions over the Amazon forest, J. Geophys. Res.-Atmos., 93, 1477–1486, https://doi.org/10.1029/JD093iD02p01477, 1988.

Jardine, K., Abrell, L., Kurc, S. A., Huxman, T., Ortega, J., and Guenther, A.: Volatile organic compound emissions from *Larrea tridentata* (creosotebush), Atmos. Chem. Phys., 10, 12191–12206, https://doi.org/10.5194/acp-10-12191-2010, 2010a.

Jardine, K. J., Sommer, E. D., Saleska, S. R., Huxman, T. E., Harley, P. C., and Abrell, L.: Gas Phase Measurements of Pyruvic Acid and Its Volatile Metabolites, Environ. Sci. Technol., 44, 2454–2460, https://doi.org/10.1021/es903544p, 2010b.

Jasper, A. W., Klippenstein, S. J., and Harding, L. B.: Secondary Kinetics of Methanol Decomposition: Theoretical Rate Coefficients for $3CH^2 + OH$, $3CH_2 + 3CH_2$, and $3CH_2 + CH_3$, J. Phys. Chem. A, 111, 8699–8707, https://doi.org/10.1021/jp0736950, 2007.

Johnston, H. S. and Heicklen, J.: Tunnelling corrections for unsymmetrical eckart potential energy barriers, J. Phys. Chem., 66, 532–533, https://doi.org/10.1021/j100809a040, 1962.

Kanakidou, M., Seinfeld, J. H., Pandis, S. N., Barnes, I., Dentener, F. J., Facchini, M. C., Van Dingenen, R., Ervens, B., Nenes, A., Nielsen, C. J., Swietlicki, E., Putaud, J. P., Balkanski, Y., Fuzzi, S., Horth, J., Moortgat, G. K., Winterhalter, R., Myhre, C. E. L., Tsigaridis, K., Vignati, E., Stephanou, E. G., and Wilson, J.: Organic aerosol and global climate modelling: a review, Atmos. Chem. Phys., 5, 1053–1123, https://doi.org/10.5194/acp-5-1053-2005, 2005.

Liebmann, J., Karu, E., Sobanski, N., Schuladen, J., Ehn, M., Schallhart, S., Quéléver, L., Hellen, H., Hakola, H., Hoffmann, T., Williams, J., Fischer, H., Lelieveld, J., and Crowley, J. N.: Direct measurement of NO_3 radical reactivity in a boreal forest, Atmos. Chem. Phys., 18, 3799–3815, https://doi.org/10.5194/acp-18-3799-2018, 2018a.

Liebmann, J. M., Muller, J. B. A., Kubistin, D., Claude, A., Holla, R., Plass-Dülmer, C., Lelieveld, J., and Crowley, J. N.: Direct measurements of NO_3 reactivity in and above the boundary layer of a mountaintop site: identification of reactive trace gases and comparison with OH reactivity, Atmos. Chem. Phys., 18, 12045–12059, https://doi.org/10.5194/acp-18-12045-2018, 2018b.

Liebmann, J., Sobanski, N., Schuladen, J., Karu, E., Hellén, H., Hakola, H., Zha, Q., Ehn, M., Riva, M., Heikkinen, L., Williams, J., Fischer, H., Lelieveld, J., and Crowley, J. N.: Alkyl nitrates in the boreal forest: formation via the NO_3-, OH- and O_3-induced oxidation of biogenic volatile organic compounds and ambient lifetimes, Atmos. Chem. Phys., 19, 10391–10403, https://doi.org/10.5194/acp-19-10391-2019, 2019.

Mellouki, A. and Mu, Y.: On the atmospheric degradation of pyruvic acid in the gas phase, J. Photoch. Photobio. A, 157, 295–300, https://doi.org/10.1016/S1010-6030(03)00070-4, 2003.

Millet, D. B., Guenther, A., Siegel, D. A., Nelson, N. B., Singh, H. B., de Gouw, J. A., Warneke, C., Williams, J., Eerdekens, G., Sinha, V., Karl, T., Flocke, F., Apel, E., Riemer, D. D., Palmer, P. I., and Barkley, M.: Global atmospheric budget of acetaldehyde: 3-D model analysis and constraints from in-situ and satellite observations, Atmos. Chem. Phys., 10, 3405–3425, https://doi.org/10.5194/acp-10-3405-2010, 2010.

Millet, D. B., Baasandorj, M., Farmer, D. K., Thornton, J. A., Baumann, K., Brophy, P., Chaliyakunnel, S., de Gouw, J. A., Graus, M., Hu, L., Koss, A., Lee, B. H., Lopez-Hilfiker, F. D., Neuman, J. A., Paulot, F., Peischl, J., Pollack, I. B., Ryerson, T. B., Warneke, C., Williams, B. J., and Xu, J.: A large and ubiquitous source of atmospheric formic acid, Atmos. Chem. Phys., 15, 6283–6304, https://doi.org/10.5194/acp-15-6283-2015, 2015.

Noodleman, L.: Valence bond description of anti-ferromagnetic coupling in transition-metal dimers, J. Chem. Phys., 74, 5737–5743, 1981.

Olivella, S., Bofill, J. M., and Solé, A.: Ab Initio Calculations on the Mechanism of the Oxidation of the Hydroxymethyl Radical by Molecular Oxygen in the Gas Phase: A Significant Reaction for Environmental Science, Chemistry, 7, 3377–3386, https://doi.org/10.1002/1521-3765(20010803)7:15<3377::AID-CHEM3377>3.0.CO;2-8, 2001.

Paulot, F., Crounse, J. D., Kjaergaard, H. G., Kroll, J. H., Seinfeld, J. H., and Wennberg, P. O.: Isoprene photooxidation: new insights into the production of acids and organic nitrates, Atmos. Chem. Phys., 9, 1479–1501, https://doi.org/10.5194/acp-9-1479-2009, 2009.

Perring, A. E., Pusede, S. E., and Cohen, R. C.: An observational perspective on the atmospheric impacts of alkyl and multifunctional nitrates on ozone and secondary organic aerosol, Chem. Rev., 113, 5848–5870, https://doi.org/10.1021/cr300520x, 2013.

Petäjä, T., Mauldin, III, R. L., Kosciuch, E., McGrath, J., Nieminen, T., Paasonen, P., Boy, M., Adamov, A., Kotiaho, T., and Kulmala, M.: Sulfuric acid and OH concentrations in a boreal forest site, Atmos. Chem. Phys., 9, 7435–7448, https://doi.org/10.5194/acp-9-7435-2009, 2009.

Praplan, A. P., Hegyi-Gaeggeler, K., Barmet, P., Pfaffenberger, L., Dommen, J., and Baltensperger, U.: Online measurements of water-soluble organic acids in the gas and aerosol phase from the photooxidation of 1,3,5-trimethylbenzene, Atmos. Chem. Phys., 14, 8665–8677, https://doi.org/10.5194/acp-14-8665-2014, 2014.

Purvis, G. D. and Bartlett, R. J.: A full coupled-cluster singles and doubles model – the inclusion of disconnected triples, J. Chem. Phys., 76, 1910–1918, https://doi.org/10.1063/1.443164, 1982.

Raber, W. H. and Moortgat, G. K.: Photooxidation of selected carbonyl compounds in air: methyl ethyl ketone, methyl vinyl ketone, methacrolein and methylglyoxal, in: Progress and problems in atmospheric chemistry, edited by: Barker, J. R., World Scientific Publishing, Singapore, 318–373, 1995.

Reed Harris, A. E., Doussin, J. F., Carpenter, B. K., and Vaida, V.: Gas-Phase Photolysis of Pyruvic Acid: The Effect of Pressure on Reaction Rates and Products, J. Phys. Chem. A, 120, 10123–10133, https://doi.org/10.1021/acs.jpca.6b09058, 2016.

Reed Harris, A. E., Cazaunau, M., Gratien, A., Pangui, E., Doussin, J.-F., and Vaida, V.: Atmospheric Simulation Chamber Studies of the Gas-Phase Photolysis of Pyruvic Acid, J. Phys. Chem. A, 121, 8348–8358, https://doi.org/10.1021/acs.jpca.7b05139, 2017a.

Reed Harris, A. E., Cazaunau, M., Gratien, A., Pangui, E., Doussin, J. F., and Vaida, V.: Atmospheric Simulation Chamber Studies of the Gas-Phase Photolysis of Pyruvic Acid, J. Phys. Chem. A, 121, 8348–8358, https://doi.org/10.1021/acs.jpca.7b05139, 2017b.

Rinne, J., Hakola, H., Laurila, T., and Rannik, Ü.: Canopy scale monoterpene emissions of *Pinus sylvestris* dominated forests, Atmos. Environ., 34, 1099–1107, https://doi.org/10.1016/S1352-2310(99)00335-0, 2000.

Roberts, J. M., Flocke, F., Chen, G., de Gouw, J., Holloway, J. S., Hübler, G., Neuman, J. A., Nicks Jr., D. K., Nowak, J. B., Parrish, D. D., Ryerson, T. B., Sueper, D. T., Warneke, C., and Fehsenfeld, F. C.: Measurement of peroxycarboxylic nitric anhydrides (PANs) during the ITCT 2K2 aircraft intensive experiment, J. Geophys. Res.-Atmos., 109, D23S21, https://doi.org/10.1029/2004jd004960, 2004.

Roiger, A., Aufmhoff, H., Stock, P., Arnold, F., and Schlager, H.: An aircraft-borne chemical ionization – ion trap mass spectrometer (CI-ITMS) for fast PAN and PPN measurements, Atmos. Meas. Tech., 4, 173–188, https://doi.org/10.5194/amt-4-173-2011, 2011.

Samanta, B. R., Fernando, R., Rösch, D., Reisler, H., and Osborn, D. L.: Primary photodissociation mechanisms of pyruvic acid on S1: observation of methylhydroxycarbene and its chemical reaction in the gas phase, Phys. Chem. Chem. Phys., 23, 4107–4119, https://doi.org/10.1039/D0CP06424F, 2021.

Sander, R., Baumgaertner, A., Cabrera-Perez, D., Frank, F., Gromov, S., Grooß, J.-U., Harder, H., Huijnen, V., Jöckel, P., Karydis, V. A., Niemeyer, K. E., Pozzer, A., Riede, H., Schultz, M. G., Taraborrelli, D., and Tauer, S.: The community atmospheric chemistry box model CAABA/MECCA-4.0, Geosci. Model Dev., 12, 1365–1385, https://doi.org/10.5194/gmd-12-1365-2019, 2019.

Schreiner, P. R., Reisenauer, H. P., Ley, D., Gerbig, D., Wu, C. H., and Allen, W. D.: Methylhydroxycarbene: Tunneling control of a chemical reaction, Science, 332, 1300–1303, https://doi.org/10.1126/science.1203761, 2011.

Shepson, P. B., Bottenheim, J. W., Hastie, D. R., and Venkatram, A.: Determination of the relative ozone and PAN deposition velocities at night, Geophys. Res. Lett., 19, 1121–1124, https://doi.org/10.1029/92gl01118, 1992a.

Shepson, P. B., Hastie, D. R., So, K. W., and Schiff, H. I.: Relationships between PAN, PPN and O_3 at urban and rural sites in ontario, Atmos. Environ. A-Gen., 26, 1259–1270, https://doi.org/10.1016/0960-1686(92)90387-z, 1992b.

Sobanski, N., Schuladen, J., Schuster, G., Lelieveld, J., and Crowley, J. N.: A five-channel cavity ring-down spectrometer for the detection of NO_2, NO_3, N_2O_5, total peroxy nitrates and total alkyl nitrates, Atmos. Meas. Tech., 9, 5103–5118, https://doi.org/10.5194/amt-9-5103-2016, 2016.

Stefan, M. I. and Bolton, J. R.: Reinvestigation of the acetone degradation mechanism in dilute aqueous solution by the UV/H_2O_2 process, Environ. Sci. Technol., 33, 870–873, https://doi.org/10.1021/es9808548, 1999.

Talbot, R., Andreae, M., Berresheim, H., Jacob, D. J., and Beecher, K.: Sources and sinks of formic, acetic, and pyruvic acids over Central Amazonia: 2. Wet season, J. Geophys. Res.-Atmos., 95, 16799–16811, https://doi.org/10.1029/JD095iD10p16799, 1990.

Vereecken, L. and Peeters, J.: The 1,5-H-shift in 1-butoxy: A case study in the rigorous implementation of transition state theory for a multirotamer system, J. Chem. Phys., 119, 5159–5170, https://doi.org/10.1063/1.1597479, 2003.

Vereecken, L., Pierloot, K., and Peeters, J.: B3LYP-DFT characterization of the potential energy surface of the $CH(X2\Pi) + C_2H_2$ reaction, J. Chem. Phys., 108, 1068–1080, https://doi.org/10.1063/1.475345, 1998.

Vesley, G. F. and Leermakers, P. A.: Photochemistry of alpha-keto acids + alpha-keto esters. 3. Photolysis of pyruvic acid in vapor phase, J. Phys. Chem., 68, 2364–2366, https://doi.org/10.1021/j100790a507, 1964.

Walker, D.: Pyruvate carboxylation and plant metabolism, Biol. Rev., 37, 215–254, https://doi.org/10.1111/j.1469-185X.1962.tb01611.x, 1962.

Wang, N., Edtbauer, A., Stönner, C., Pozzer, A., Bourtsoukidis, E., Ernle, L., Dienhart, D., Hottmann, B., Fischer, H., Schuladen, J., Crowley, J. N., Paris, J.-D., Lelieveld, J., and Williams, J.: Measurements of carbonyl compounds around the Arabian Peninsula: overview and model comparison, Atmos. Chem. Phys., 20, 10807–10829, https://doi.org/10.5194/acp-20-10807-2020, 2020.

Wang, S. Y., Hornbrook, R. S., Hills, A., Emmons, L. K., Tilmes, S., Lamarque, J. F., Jimenez, J. L., Campuzano-Jost, P., Nault, E. A., Crounse, J. D., Wennberg, P. O., Kim, M., Allen, H., Ryerson, T. B., Thompson, C. R., Peischl, J., Moore, F., Nance, D., Hall, B., Elkins, J., Tanner, D., Huey, L. G., Hall, S. R., Ullmann, K., Orlando, J. J., Tyndall, G. S., Flocke, F. M., Ray, E., Hanisco, T. F., Wolfe, G. M., St Clair, J., Commane, R., Daube, B., Barletta, B., Blake, D. R., Weinzierl, B., Dollner, M., Conley, A., Vitt, F., Wofsy, S. C., Riemer, D. D., and Apel, E. C.: Atmospheric acetaldehyde: importance of air-sea exchange and a missing source in the remote troposphere, Geophys. Res. Lett., 46, 5601–5613, https://doi.org/10.1029/2019gl082034, 2019.

Williams, J., Crowley, J., Fischer, H., Harder, H., Martinez, M., Petäjä, T., Rinne, J., Bäck, J., Boy, M., Dal Maso, M., Hakala, J., Kajos, M., Keronen, P., Rantala, P., Aalto, J., Aaltonen, H., Paatero, J., Vesala, T., Hakola, H., Levula, J., Pohja, T., Herrmann, F., Auld, J., Mesarchaki, E., Song, W., Yassaa, N., Nölscher, A., Johnson, A. M., Custer, T., Sinha, V., Thieser, J., Pouvesle, N., Taraborrelli, D., Tang, M. J., Bozem, H., Hosaynali-Beygi, Z., Axinte, R., Oswald, R., Novelli, A., Kubistin, D., Hens, K., Javed, U., Trawny, K., Breitenberger, C., Hidalgo, P. J., Ebben, C. J., Geiger, F. M., Corrigan, A. L., Russell, L. M., Ouwersloot, H. G., Vilà-Guerau de Arellano, J., Ganzeveld, L., Vogel, A., Beck, M., Bayerle, A., Kampf, C. J., Bertelmann, M., Köllner, F., Hoffmann, T., Valverde, J., González, D., Riekkola, M.-L., Kulmala, M., and Lelieveld, J.: The summertime Boreal forest field measurement intensive (HUMPPA-COPEC-2010): an overview of meteorological and chemical influences, Atmos. Chem. Phys., 11, 10599–10618, https://doi.org/10.5194/acp-11-10599-2011, 2011.

Yamamoto, S. and Back, R. A.: The photolysis and thermal-decomposition of pyruvic-acid in the gas-phase, Can. J. Chem., 63, 549–554, https://doi.org/10.1139/v85-089, 1985.

Zhao, Y. and Truhlar, D. G.: The M06 suite of density functionals for main group thermochemistry, thermochemical kinetics, noncovalent interactions, excited states, and transition elements: two new functionals and systematic testing of four M06-class functionals and 12 other functionals, Theor. Chem. Account., 120, 215–241, https://doi.org/10.1007/s00214-007-0310-x, 2008.